Trajectory Design for Lagrange Point Missions using DST in Restricted Three-Body Problem

Yoshihide SUGIMOTO

In Partial Fulfillment of the Requirements
for the Degree of
Doctor of Philosophy

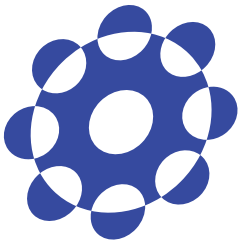

Department of Space and Astronautical Science
School of Physical Sciences
The Graduate University for Advanced Studies
2014

Acknowledgments

I thank Associate Professor Yasuhiro Kawakatsu, Institute of Space and Astronautical Science (ISAS)/ Japan Aerospace Exploration Agency (JAXA), and Assistant Professor Takanao Saiki, ISAS/ JAXA, for supervise this study and allowing me to learn significant knowledge for the space mission design. Thanks go to Mrs. Ruriko Kinoshita for her assistance in research environment. I would like to thank the Japan Society for the Promotion of Science (Japan) for financial support during this study.

I thank Dr. Stefano Campagnola, Dr. Chit Hong Yam for giving me professional insight into this research and Mr. Federico Zuiani and all students from Kawakatsu and Kawaguchi Laboratories for their kind support.

Finally, special thanks to my wife and parents. They give me ungrudging support to finalize this thesis.

Contents

List of Figures

List of Tables

CHAPTER 1

Introduction

Contents

1.1 Research Background

In the restricted three-body problem, there are five equilibrium points so called Lagrangian points (or simply L points) that maintain their position with respect to two dominant bodies described as *primaries*. Once an infinitesimal particle, *i.e.* third body, is putted at one of the L points, the bird body will keep the location on the point. Particularly, the collinear Lagrangian points have attracted historical interest for space mission because of their suitable location. However, the collinear L points and orbits around that L points are well known as unstable and, therefore, the frequent stationkeeping maneuver is required to keep the spacecraft nearby the reference L point.

In the present, several missions have been operated around collinear Lagrangian points in Sun-Earth-spacecraft restricted three-body problem. The spacecraft inserted on the collinear L points keep its position collinear with respect to the primaries. In particular, two of three Lagrange point Sun-Earth (SE) L1 and L2 are considered as a suitable location for space based missions like deep-space observations. Table 1.1 presents the past, current and future SE L1 and L2 points missions. Thanks to the success of past and current missions, the SE L2 point is becoming more and more attractive location for the missions. The L3 is another collinear L point, but since its position is opposite to the Sun from Earth, the environment around L3 is severe and not very appropriate for mission operations.

Table 1.1: Lagrangian Point Missions

Mission	SE-L1	SE-L2
Current & Past	ISEE-3 [1978] WIND [1994] SOHO [1996] ACE [1997] Genesis [2001]	WMAP [2001] Planck [2009] Herschel [2009] Chang'e-2 [2010] Gaia [2013]
Future	LISA Pathfinder [2015]	Spektr-RG [2015] JWST [2018] Euclid [2020] SPICA [2022]

The SE L1 and L2 are in the spotlight also for the deep-space port operational orbit since their location is out of Earth's sphere of influence (SOI) and opens to the deep-space, allowing easy access from interplanetary trajectories. Recently, Hamasaki showed the effectiveness of the transfer from the deep-space port around the SE-L2 in his research [Hamasaki 2013] to access specific asteroid targets. Since, the deep-space port assumed around the L2 is already outside of the Earth's SOI, it enables an efficient deep-space missions that could be explored by the low thrust propulsion system.

Three dimensional, periodic Halo orbits are found around the collinear L-points in the Circular Restricted Three-Body Problem (CR3BP). The CR3BP is an approximated model that is commonly used for preliminary mission design. The CR3BP is a symmetry and autonomous model since the two dominant bodies rotate on circular orbits about their barycenter. Dr. Robert W. Farquhar found the Halo orbits analytically and named in his Ph.D. thesis [Faquhar 1968] and Dr. Kathleen Howell showed the precise numerical design for the Halo orbits [K.C. 1984]. The halo orbits are attractive orbit since their periodicity and location, however, the collinear L-points are well known as unstable equilibrium points, therefore, the orbital stability around those points have been studied in past decades.

Figure 1.1 presents an example of Halo orbits designed in Sun-Earth (SE) CR3BP. The blue and red symbols show Earth and the L2 point, respectively. The reference frame is considered as a rotating frame whose origin lies at the Sun-Earth's barycenter, with the x axis directing towards the Earth, the z axis is normal to the primaries' orbital plane and y axis is

defined by the right hand law. In this rotating frame, Hallo orbits draw an ellipse in a counter clockwise. It can be observed that the orbit rotate around the L2 and since the orbit is periodic the motion will repeat forever.

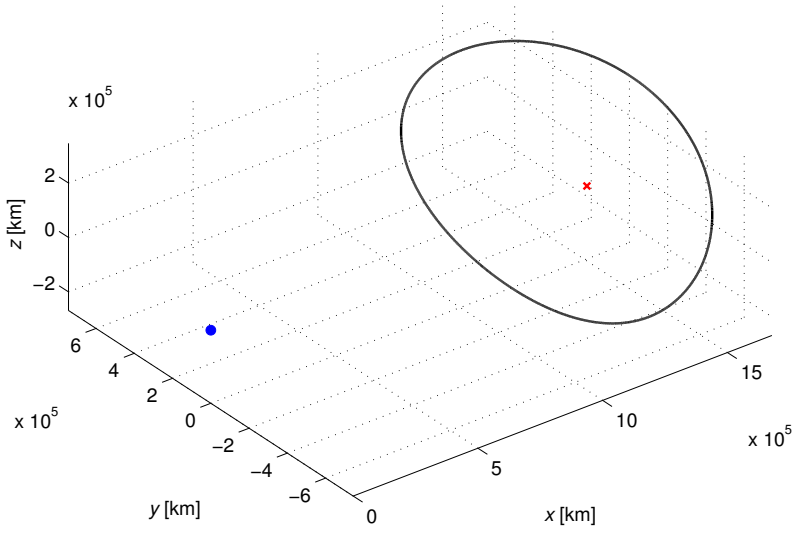

Figure 1.1: Halo Orbit around Sun–Earth L2

The libration point orbits are, however, highly unstable as mentioned before and the flight operation requires frequent stationkeeping maneuver in order to keep the spacecraft on the reference trajectory. The effective stationkeeping problem is considered for the existing actual missions [Dunham 2001]. Howell and Pernicka [K.C. 1993] investigated the stationkeeping problem by allowing torus centered motion about the nominal reference. For more sophisticated stationkeeping problem, Scheeres [Scheeres 2003] has worked stabilizing the unstable orbit motion by means of Dynamical Systems Theory (DST) in Hill's equation of motions. The invariant manifolds are obtained by means of the Floquet theory which gives the principal motion about the reference trajectory by applying the Linearlized State Transition Matrix (STM). Figure 1.2 presents an example of the manifolds with respect to a specific Halo orbit expressed as a black curve in Earth center rotating reference frame. The green curves represent natural converging trajectories (stable manifold) and the red curves show the natural diverging trajectories (unstable manifold).

Genesis is the first mission whose trajectory was design by using the DST. The trajectory design application of the DST to an actual mission has

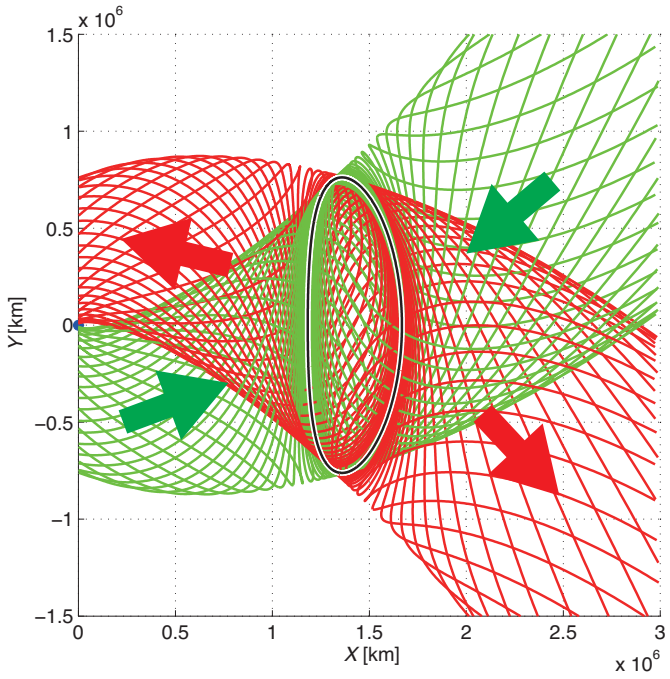

Figure 1.2: Stable and Unstable Manifolds of the Halo Orbit

been studied and shown by Koon, Lo, Marsden and Ross [Koon 1999], [Koon 2000]. Nakamiya [Nakamiya 2011] exploited the stable manifold for the transfer trajectory design to the Halo orbits around SE L2. In result, a transfer trajectory designed by the stable manifold can avoid significant and sensitive Halo orbit insertion maneuver. This is extremely useful for the orbit insertion into highly sensitive orbits like the one around collinear Lagrangian points.

The practical orbit maintenance method by means of the DST has been surveyed by Nakamiya [Nakamiya 2010] in the CR3BP. Theoretically, only the diverging subspace, *i.e.* unstable manifold, make the orbit displacement grow from the nominal reference orbit. However, the CR3BP is a simplified dynamic model that assumes ideal physical geometries Furthermore, the Halo orbits are designed only in the autonomous model (CR3BP) in strict definition and periodic orbit design is very hard in more actual model than CR3BP because the actual model is no more a autonomous model what has the time independency and several perturbing sources like orbit eccentricity or gravity perturbation. This fact make the maneuver design complicated and there is no brief report for the orbit maintenance in actual dynamics. The orbital maintenance maneuver along with reference trajectories designed in the actual model is important and essential for long-time mission operation like long lifetime observation and space port.

The Elliptic Restricted Three-Body Problem (ER3BP) is employed for the higher fidelity dynamical model. The ER3BP includes the orbit eccentricity of the two primaries which is assumed as zero in the CR3BP. Generally the primaries are rotating on the elliptic orbit with a specific orbit eccentricity. Hence, the ER3BP is a more general dynamic model of the three-body problem.

Previously, the study on periodic orbit design in the ER3BP has been investigated. Szebehely [Szebehely 1967] worked detail description of the basic equation of motion of the elliptic three-body problem and showed the sufficient conditions for the periodic orbit in elliptic problem. Broucke [Broucke 1969] investigated the systematic periodic orbit design in the two-dimensional ER3BP based on Szebehely's work. He found the family of periodic solutions in two-dimensional ER3BP for all ranges of eccentricity and mass ratios. In recent studies, Sarris [Sarris 1989] and Campagnola, Lo and Newton [Campagnola 2008] have extended the two-dimensional work to the three-dimensional ER3BP. The periodic orbits provided in previous studies have been done with short periods and some of them are not elliptic in rotating reference unlike Halo orbits. The long period of orbit design is technically difficult compared to the short period of orbit and it has not been well studied. The orbit shape is depends on the orbit period and, therefore, the past studies have a limit on the orbit shape.

1.2 Objectives

This study has worked through the application of the reference orbit design and maintenance under a higher fidelity model than CR3BP. The reference orbit design method is provided at first and the DST is considered for the designed reference trajectory in order to prove the effectiveness of the maintenance maneuver design.

In ER3BP periodic orbits in vicinity of the L2 point are designed as reference. The periodic orbits are constrained nearby reference Halo orbits given by results of orbital design in the CR3BP. Thus the orbit will not be of a random shape but an elliptic orbit in the rotating reference coordinate similar to Halo orbits. Some of the periodic orbits require a large number of revolutions to reproduce the initial condition, which also requires long term of the very accurate trajectory propagation. In that case, the orbits are divided into smaller number of revolutions until getting a reasonable design condition and then, the decided trajectory components are connected to realize full revolution orbit.

The effective maintenance maneuver design is obtained by loosing correction constraint. Usually, the determined actual trajectory are to be modified onto the reference trajectory, however, only the diverging component in the orbit deviation is treated to stay close to the reference trajectory. The benefit from the solution of eigenvalue problem for the Monodromy matrix, which is the State Transition Matrix (STM) along periodic orbit, the principal subspaces are derived about the reference. The diverging subspace is only error stretching direction in the state displacement. Therefore, when the diverging component is nullified, the deviation will not increase and stay around the reference trajectory.

1.3 Thesis Framework

This thesis investigates the trajectory design in realistic restricted three-body problem. The first half introduces the dynamical model and trajectory design in approximated dynamical model. The later half expands the methodology to the more actual model.

Chapter 2 leads the equations of motion both for the CR3BP and the ER3BP. The CR3BP is mainly used for the establishment of the trajectory deign method. The ER3BP considers orbit eccentricity of two primaries. Therefore, the model remains the generality but more realistic than the CR3BP.

Chapter 3 shows the Halo orbit design in the CR3BP. The Halo orbits are known as three-dimensional, periodic orbit around the collinear Lagrangian points. The orbits have been well studied in past research. The designed Halo orbits' initial conditions are very useful for the initial estimation of periodic orbit design in actual model.

Chapter 4 introduces the contribution of the DST to trajectory design. The feasible orbit maintenance method by suppressing the diverging subspace is shown. The invariant manifolds constructed in the DST are very useful structure and give us a lot of information for the reference orbit. The diverging subspace is a maximum error stretching direction. The state displacement will grow only along the direction. Hence, the state displacement canceled out the direction will stay close to the reference orbit.

Chapter 5 to **Chapter 6** shows the periodic orbit design in the ER3BP. The periodic orbit is divided in short period and long period orbits. The short period orbits are designed in straightforward by the nu medical differential correction. The long period orbit needs the special technique for the design and the method is presented.

Chapter 7 expand the trajectory design using the DST in the ER3BP. In the CR3BP, the basic idea and the usefulness are shown. Therefore, this chapter mainly presents the difference from the normally used maneuver design and the effectiveness of the application.

CHAPTER 2

Dynamics Model

Contents

2.1 Restricted Three-Body Problem

This chapter introduces the restricted three-body problem's equation of motion. For the first, the Circular Restricted Three-Body Problem (CR3BP) is considered and the Elliptic Restricted Three-Body Problem (ER3BP) is brought in next.

In order to design trajectories of spacecraft, the solution of two-body problem is commonly used as the starting point for more complex study. The two-body problem is sufficient to give fundamental insights of the spacecraft motion and analyse the mission. However, the two-body problem is incomplete to predict more complex motion around particular region like equilibrium point. The usage of three-body problem is then taken into account. In contrast to the two-body problem, the general three-body problem does not have an analytical solution. Thus, the simplified model for the three-body problem are studied and the restricted three-body problem is one simple analytical solution.

A mass of spacecraft is negligible compared with those of two dominant bodies (primaries). Hence, the gravity acceleration induced by a spacecraft is assumed zero to the primaries. Figure 2.1 compares the difference between the general three-body problem and the restricted three-body problem.

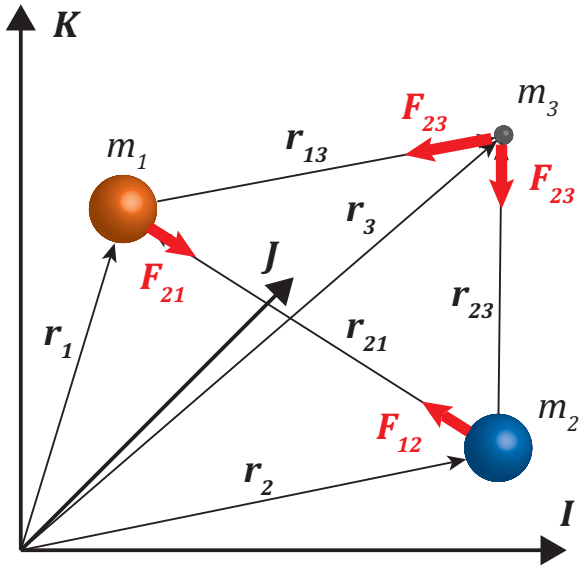

Figure 2.1: Geometry for the Restricted Three-Body Problem

2.2 Circular Restricted Three-Body Problem

The certain simplifying assumptions for the restricted three-body problem can be made attempting to characterize the motion. The Circular Restricted Three-Body Problem (CR3BP) is the simplified model commonly used for the restricted three-body problem. This problem makes two simplifying assumptions:

1. Mass of the third body is negligible

2. Primaries move in circular orbits about the center of mass

Generally, the planets, satellites and asteroids orbits are elliptic orbits with small eccentricity. For instance, the eccentricity of Earth orbit about Sun is approximately 0.0167 and the Moon about Earth is known as 0.0549. They are small enough to be regarded as the circular orbit and, therefore, the CR3BP is a well approximated model for general studies of the trajectory design.

Consider a non-inertial, co-moving rotating frame of reference xyz whose origin lies as the barycenter G of the two-body system, with the x-axis directed towards the secondary body (see in Figure 2.2). The y-axis lies in the orbital plane, to which the z-axis is normal to the plane. In this rotating reference frame, the primaries are always on the x-axis keeping the mutual distance D constant.

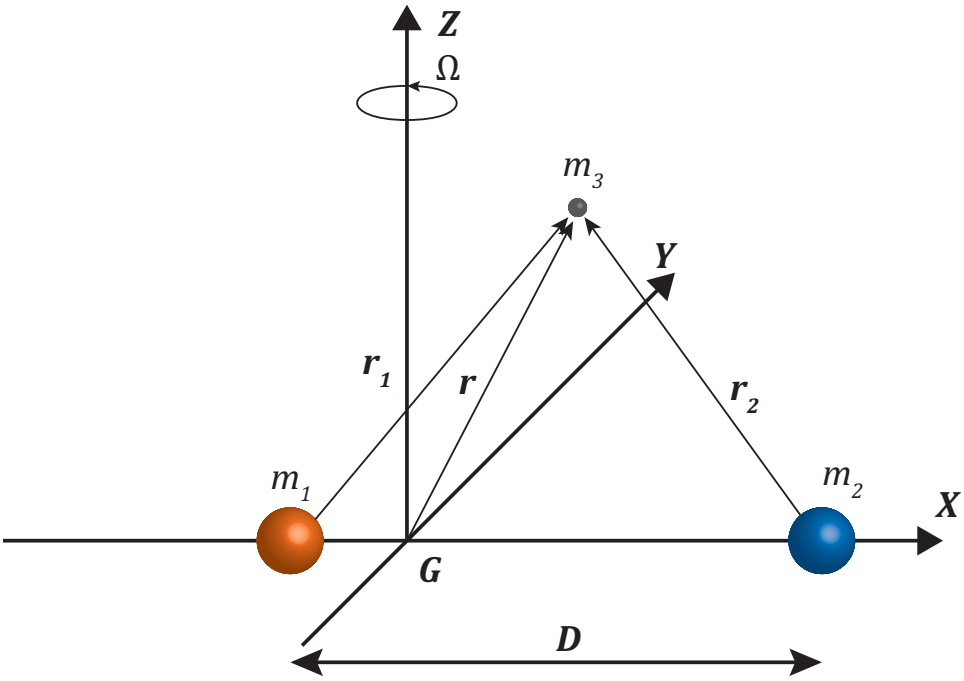

Figure 2.2: Rotating Reference Frame for CR3BP

In the rotating reference frame, the position vector of m relative to the barycenter is given by:

$$\mathbf{R} = \mathrm{X}\hat{\mathbf{i}} + \mathrm{Y}\hat{\mathbf{j}} + \mathrm{Z}\hat{\mathbf{k}} \tag{2.1}$$

The position of m relative to m_1 and m_2 are:

$$\mathbf{R}_1 = (\mathrm{X} - \mathrm{X}_1)\hat{\mathbf{i}} + \mathrm{Y}\hat{\mathbf{j}} + \mathrm{Z}\hat{\mathbf{k}} \tag{2.2}$$

$$\mathbf{R}_2 = (\mathrm{X} - \mathrm{X}_2)\hat{\mathbf{i}} + \mathrm{Y}\hat{\mathbf{j}} + \mathrm{Z}\hat{\mathbf{k}} \tag{2.3}$$

where X_1 and X_2, the position of m_1 and m_2, are given in terms of the mass ratio of m_1 and m_2, π_1 and π_2, respectively:

$$\mathrm{X}_1 = -\pi_2 \mathrm{D} \tag{2.4}$$

$$\mathrm{X}_2 = \pi_1 \mathrm{D} \tag{2.5}$$

Since the reference frame is rotating, the time derivative of the unit vectors $\hat{\mathbf{i}}$ and $\hat{\mathbf{j}}$ are not zero. The inertial angular velocity $\boldsymbol{\Omega}$ is:

$$\boldsymbol{\Omega} = \Omega\hat{\mathbf{k}} \tag{2.6}$$

where,

$$\Omega = \sqrt{\frac{\mu_1 + \mu_2}{\mathrm{D}^3}}\hat{\mathbf{k}} \tag{2.7}$$

Therefore, the time derivative of the position vector in the rotating frame is:

$$\dot{\mathbf{R}} = \mathbf{v}_{\mathrm{G}} + \boldsymbol{\Omega} \times \mathbf{R} + \mathbf{v}_{\mathrm{rel}} \tag{2.8}$$

where $\mathbf{v}_{\mathrm{G}}$ is the inertial velocity and $\mathbf{v}_{\mathrm{rel}}$ is the velocity vector in the rotating reference frame, namely,

$$\mathbf{v}_{\mathrm{rel}} = \dot{\mathrm{X}}\hat{\mathbf{i}} + \dot{\mathrm{Y}}\hat{\mathbf{j}} + \dot{\mathrm{Z}}\hat{\mathbf{k}} \tag{2.9}$$

The absolute acceleration of m is derived from Eq. 2.8 as:

$$\ddot{\mathbf{R}} = \mathbf{a}_{\mathrm{G}} + \dot{\boldsymbol{\Omega}} \times \mathbf{R} + \boldsymbol{\Omega} \times (\boldsymbol{\Omega} \times \mathbf{R}) + 2\boldsymbol{\Omega} \times \mathbf{v}_{\mathrm{rel}} + \mathbf{a}_{\mathrm{rel}} \tag{2.10}$$

Similar to $\mathbf{v}_{\mathrm{rel}}$, the inertial acceleration $\mathbf{a}_{\mathrm{rel}}$ is given:

$$\mathbf{a}_{\mathrm{rel}} = \ddot{\mathrm{X}}\hat{\mathbf{i}} + \ddot{\mathrm{Y}}\hat{\mathbf{j}} + \ddot{\mathrm{Z}}\hat{\mathbf{k}} \tag{2.11}$$

Recall from the assumption of CR3BP described in beginning of this section, the inertial velocity $\mathbf{v}_{\mathrm{G}}$ and angular velocity $\boldsymbol{\Omega}$ are constant. Hence, $\mathbf{a}_{\mathrm{G}}$ and $\dot{\boldsymbol{\Omega}}$ become zero and the Eq. 2.10 is deformed:

$$\ddot{\mathbf{R}} = \boldsymbol{\Omega} \times (\boldsymbol{\Omega} \times \mathbf{R}) + 2\boldsymbol{\Omega} \times \mathbf{v}_{\mathrm{rel}} + \mathbf{a}_{\mathrm{rel}} \tag{2.12}$$

Substituting Eqs. 2.1 and 2.6 into Eq.2.12 yields:

$$\ddot{\mathbf{R}} = (\ddot{\mathrm{X}} - 2\Omega\dot{\mathrm{Y}} - \Omega^2\mathrm{X})\hat{\mathbf{i}} + (\ddot{\mathrm{Y}} + 2\Omega\dot{\mathrm{X}} - \Omega^2\mathrm{Y})\hat{\mathbf{j}} + \ddot{\mathrm{Z}}\hat{\mathbf{k}} \tag{2.13}$$

We obtain an expression for the inertial acceleration in terms of coordinate value expressed in the rotating reference frame. Now that Newton's second law of motion for the third body is:

$$\mathrm{m}\ddot{\mathbf{R}} = \mathbf{F}_1 + \mathbf{F}_2 \tag{2.14}$$

$\mathbf{F}_1$ and $\mathbf{F}_2$ are external force on m induced by the gravity from m_1 and m_2.

$$\begin{aligned} \mathbf{F}_1 &= -\frac{\mu_1 \mathrm{m}}{\mathrm{R}_1^3}\mathbf{R}_1 \\ \mathbf{F}_2 &= -\frac{\mu_2 \mathrm{m}}{\mathrm{R}_2^3}\mathbf{R}_2 \end{aligned} \tag{2.15}$$

Substituting Eq. 2.15 into Eq. 2.14 and dividing by m yields:

$$\ddot{\mathbf{R}} = -\frac{\mu_1}{\mathrm{R}_1^3}\mathbf{R}_1 - \frac{\mu_2}{\mathrm{R}_2^3}\mathbf{R}_2 \tag{2.16}$$

Finally, substituting Eqs. 2.4 and 2.5 into Eq. 2.16 and, then, equating the coefficients of $\hat{\mathbf{i}}$, $\hat{\mathbf{j}}$ and $\hat{\mathbf{k}}$ of the resulting equation and Eq. 2.13 derives the three scaler equations of motion for the CR3BP:

$$\ddot{\mathrm{X}} - 2\Omega\dot{\mathrm{Y}} - \Omega^2\mathrm{X} = -\frac{\mu_1}{\mathrm{R}_1^3}(\mathrm{X} + \pi_2\mathrm{D}) - \frac{\mu_2}{\mathrm{R}_2^3}(\mathrm{X} - \pi_1\mathrm{D}) \tag{2.17}$$

$$\ddot{\mathrm{Y}} + 2\Omega\dot{\mathrm{X}} - \Omega^2\mathrm{Y} = -\frac{\mu_1}{\mathrm{R}_1^3}\mathrm{Y} - \frac{\mu_2}{\mathrm{R}_2^3}\mathrm{Y} \tag{2.18}$$

$$\ddot{\mathrm{Z}} = -\frac{\mu_1}{\mathrm{R}_1^3}\mathrm{Z} - \frac{\mu_2}{\mathrm{R}_2^3}\mathrm{Z} \tag{2.19}$$

2.2.1 Normalization

In order to make the numerical value in friendly form, the equations are to be normalized.

The total mass of the primaries is given. In addition, by means of the assumption of the CR3BP, the distance between two primaries, D, and the angular velocity of the reference frame, Ω are constant. Therefore, normalizing the total mass, D and Ω gives the CR3BP equation of motions in simpler form:

$$\ddot{\mathrm{x}} - 2\dot{\mathrm{y}} - \mathrm{x} = -\frac{\pi_1}{\mathrm{r}_1^3}(\mathrm{x} + \pi_2) - \frac{\pi_2}{\mathrm{r}_2^3}(\mathrm{x} - \pi_1) \tag{2.20}$$

$$\ddot{\mathrm{y}} + 2\dot{\mathrm{x}} - \mathrm{y} = -\frac{\pi_1}{\mathrm{r}_1^3}\mathrm{y} - \frac{\pi_2}{\mathrm{r}_2^3}\mathrm{y} \tag{2.21}$$

$$\ddot{\mathrm{z}} = -\frac{\pi_1}{\mathrm{r}_1^3}\mathrm{z} - \frac{\pi_2}{\mathrm{r}_2^3}\mathrm{z} \tag{2.22}$$

2.3 Elliptic Restricted Three-Body Problem

The Elliptic Restricted 3-Body Problem (ER3BP) is more actual dynamical model than CR3BP. The ER3BP is a dynamical model with the co-orbiting primaries orbiting on elliptic orbits. The eccentricity of actual two-body systems are commonly very small but not zero and the small eccentricity may not be negligible. The initial condition of trajectory designed in the CR3BP is not often sufficient for the full ephemeris model. The definition of reference frame is rotating xyz coordinate like CR3BP (see Figure 2.3)

but since the primaries are rotating on elliptic orbits, the distance between the primaries and the angular velocity of the reference frame.

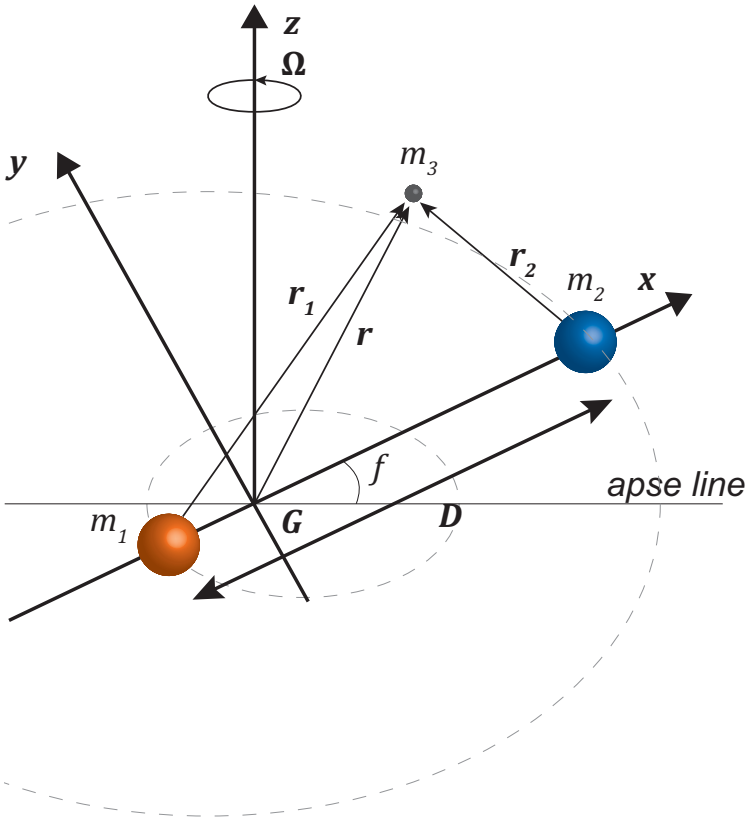

Figure 2.3: Rotating Reference Frame for ER3BP

The mutual distance between primaries is normalized to 1 at the instantaneous position in the ER3BP. In order to normalize and reconstruct the equation of motion for ER3BP, the solution to the elliptic orbit in two-body problem in polar coordinate is utilized which gives the following relations:

$$\mathrm{d}(\mathrm{f}) = \frac{1}{1 + \mathrm{e}\cos\mathrm{f}} \tag{2.23}$$

$$\mathrm{d}^2\dot{\mathrm{f}} = 1 \tag{2.24}$$

$$\ddot{\mathrm{d}} = \mathrm{d}\dot{\mathrm{f}}^2 - \frac{1}{\mathrm{r}^2} \tag{2.25}$$

Differentiating Eq. 2.24 with respect to time and solving for $\dot{\mathrm{d}}$ gives:

$$\dot{\mathrm{d}} = -\frac{\ddot{\mathrm{df}}}{2\dot{\mathrm{f}}} \tag{2.26}$$

Substituting Eq. 2.24 into Eqs. 2.25 and 2.26 yields:

$$\ddot{\mathrm{d}} = \frac{1}{\mathrm{r}^3} - \frac{1}{\mathrm{d}^2} \tag{2.27}$$

$$\dot{\mathrm{d}} = -\frac{\mathrm{d}^3\ddot{\mathrm{f}}}{2} \tag{2.28}$$

Expressing the position in the complex vector $\xi = \mathrm{x} + \mathrm{iy}$, then the position of m can be written as:

$$\mathbf{r} = \xi \mathrm{d}\, \exp(\mathrm{if}) \tag{2.29}$$

When the complex position vectors of m with respect to the primaries m_1 and m_2 are described in $\mathbf{r}_1^*$ and $\mathbf{r}_2^*$, the gravitational acceleration induced by the primaries is shown:

$$\ddot{\mathbf{r}} = (-\frac{\pi_1 \mathbf{r}_1^*}{|\mathrm{r}_1^*|^3} - \frac{\pi_2 \mathbf{r}_2^*}{|\mathrm{r}_2^*|^3})\exp(\mathrm{if}) \tag{2.30}$$

$$= (-\frac{\pi_1(\xi + \pi_2)}{|\xi + \pi_2|^3} - \frac{\pi_2(\xi - \pi_1)}{|\xi - \pi_1|^3})\frac{\exp(\mathrm{if})}{\mathrm{d}^2} \tag{2.31}$$

Now the forces in inertial frame is derived in terns of the position vector in rotating coordinate ξ. The term $\exp(\mathrm{if})$, right hand side of Eq. 2.31, illustrates the transformation from rotating pulsating coordinate to non-rotating inertial frame. Let simplify the Eq. 2.31 by introducing term of external force:

$$\mathbf{F}(\xi) = \frac{\pi_1(\xi + \pi_2)}{|\xi + \pi_2|^3} - \frac{\pi_2(\xi - \pi_1)}{|\xi - \pi_1|^3} \tag{2.32}$$

then,

$$\ddot{\mathbf{r}} = \mathbf{F}(\xi)\frac{\exp(\mathrm{if})}{\mathrm{d}^2} \tag{2.33}$$

Solving Eq. 2.33 with Eq. 2.29 expanded until second derivative for $\ddot{\mathbf{r}}$ yields:

$$\mathbf{F}(\xi)\frac{\exp(\mathrm{if})}{\mathrm{d}^2} = \mathrm{A}\exp(\mathrm{if})(\ddot{\mathrm{d}}\xi + 2\dot{\mathrm{d}}\dot{\xi} + 2\mathrm{i}\dot{\mathrm{f}}\dot{\mathrm{d}}\xi + 2\mathrm{i}\dot{\mathrm{f}}\mathrm{d}\dot{\xi} + \mathrm{d}\ddot{\xi} + \mathrm{i}\ddot{\mathrm{f}}\mathrm{d}\xi - \dot{\mathrm{f}}^2\mathrm{d}\xi) \tag{2.34}$$

Multiplying by $d^3 \exp(-if)$ for both side of Eq. 2.34 and using Eqs. 2.24, 2.27 and 2.28

$$d\mathbf{F}(\xi) = -d\xi - \ddot{f}d^6\dot{\xi} + 2id^2\dot{\xi} + d^4\ddot{\xi} \tag{2.35}$$

Since the true anomaly of the primaries is independent variable, the relation between the time derivatives of ξ with respect to f becomes:

$$\dot{\xi} = \frac{d\xi}{df}\dot{f} \tag{2.36}$$

$$\ddot{\xi} = \frac{d^2\xi}{df^2}\dot{f}^2 + \frac{d\xi}{df}\ddot{f} \tag{2.37}$$

Substituting Eqs. 2.36 and 2.37 into Eq. 2.35 we get:

$$(\xi + \mathbf{F}(\xi))r = \frac{d^2\xi}{df^2} + 2i\frac{d\xi}{df} \tag{2.38}$$

Equating the real and imaginary terms of the both sides of Eq. 2.38 and apply the expression of $d(f)$ summarizes the equations of motion for the planer ER3BP:

$$\ddot{x} - 2\dot{y} = \frac{\partial U}{\partial x}(1 + e\cos f)^{-1} \tag{2.39}$$

$$\ddot{y} + 2\dot{x} = \frac{\partial U}{\partial y}(1 + e\cos f)^{-1} \tag{2.40}$$

where,

$$U = \frac{x^2 + y^2}{2} + \frac{\pi_1}{r_1} + \frac{\pi_2}{r_2} + \frac{\pi_1\pi_2}{2} - \frac{\pi_1\pi_2}{2} \tag{2.41}$$

We need to solve also for z in order to expand the equations of motion in three dimensional fashion. While the z coordinate does not take place in the transformation involving the rotation around the z-axis because it is independent to non-uniform rotation angular velocity. Hence, it is made dimensionless only by the variable mutual distance between the primaries. Therefore, the effective potential for three dimensional problem is:

$$\begin{aligned} U &= (U_C - \frac{1}{2}(1 + e\cos f)z^2)(1 + e\cos f)^{-1} \\ &= [\frac{1}{2}(x^2 + y^2 - e\cos f\, z^2) - \frac{\pi_1}{r_1^3}\mathbf{r}_1 - \frac{\pi_2}{r_2}\mathbf{r}_2 - \frac{\pi_1\pi_2}{2}] \\ &\quad (1 + e\cos f)^{-1} \end{aligned} \tag{2.42}$$

Therefore, the equations of motion of the third body for three dimensional problem are:

$$\ddot{x} - 2\dot{y} = \frac{\partial U_C}{\partial x} - \frac{e\cos f}{1+e\cos f}\frac{\partial U_E}{\partial x} \tag{2.43}$$

$$\ddot{y} + 2\dot{y} = \frac{\partial U_C}{\partial y} - \frac{e\cos f}{1+e\cos f}\frac{\partial U_E}{\partial y} \tag{2.44}$$

$$\ddot{z} = \frac{\partial U_C}{\partial z} - \frac{e\cos f}{1+e\cos f}\frac{\partial U_E}{\partial z} \tag{2.45}$$

where

$$U_E = U + z^2/2 \tag{2.46}$$

represents the effective potential specifically the elliptic problem. In Eqs. 2.44, 2.45 and 2.45 we divide the acceleration related to eccentricity and when the eccentricity becomes zero, the second terms of the right side of the equations are canceled out and the equations are equal to CR3BP. Therefore, the ER3BP is more actual model than CR3BP and is a general model of restricted three-body problem.

CHAPTER 3

Periodic Orbits in CR3BP

Contents

3.1 Lagrangian Points

In the restricted three-body problem, five equilibrium points are calculated. At such points, the gravitational forces and the centrifugal force affecting on the third body are balanced. Therefore, theoretically, once a particle (small body) is putted on one of the point, the particle keeps the location at the point. The equations of motion in the CR3BP are provided as Eqs. 2.20 - 2.22. Setting all the derivatives to zero in the equation, we can nullify the velocity and the acceleration components. The solution of the resulting equations gives the equilibrium points. Euler discovered three collinear equilibrium points, L_1 to L_3, which exist on the x-axis and Lagrange solved two other points called equilateral points, L_4 and L_5. Figure 3.1 shows the configuration of the L points. The axis definition is same as shown in Figure 2.2. Those five equilibrium points are called libration points or Lagrangian points (L points).

In a certain case, when we assume the dominant bodies as Sun and Earth for primary and secondary bodies, respectively, the location of the L points are presented in Table 3.1.

Among these five Lagrangian points, three collinear points, L_1-L_3, are known as saddle point (unstable equilibrium point). Hence, in order to keep the spacecraft neighbor to these points, it is required that the precise orbit design.

Lissajous and Halo orbits are well known as the orbit around collinear L points. Especially, Halo orbits are closed orbit and, therefore, they attract particular attention.

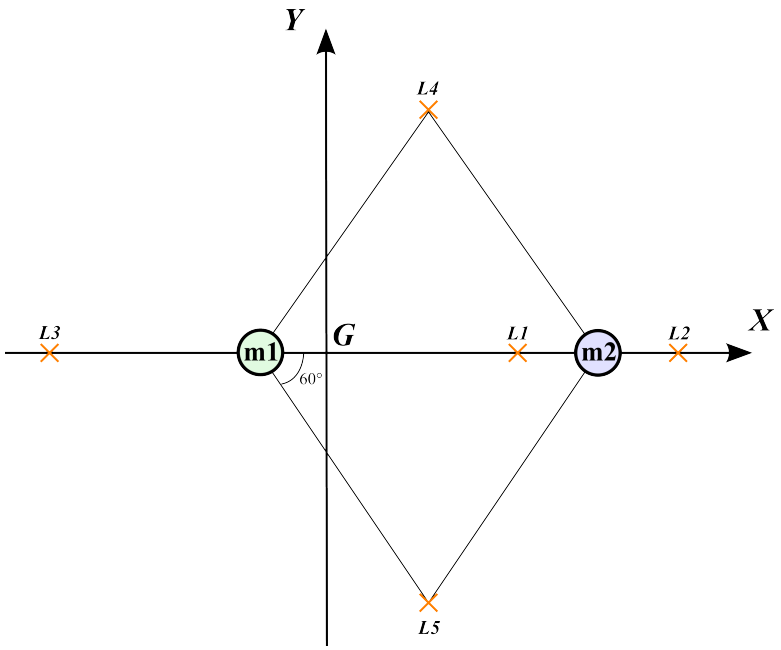

Figure 3.1: Lagrangian Points

Table 3.1: Location of Sun Earth Lagrangian Points

Points	X [km]	Y [km]	Z [km]
L_1	1.48×10^8	0	0
L_2	1.51×10^8	0	0
L_3	-1.50×10^8	0	0
L_4	0.748×10^8	1.30×10^8	0
L_5	0.748×10^8	-1.30×10^8	0

3.2 Halo Orbits

Halo orbits are periodic, three dimensional and elliptic orbits which exist around the collinear Lagrangian points designed in the CR3BP. As shown in Figure 1.1 the Halo orbits rotate around the Lagrangian point periodically in rotating reference. The Halo orbits exist around the Lagrangian point with various shape and this research identifies the size of halo orbit as amplitude of out plane motion A_z.

The motion in the CR3BP shows symmetry with respect to two different basis as:

$$(\mathrm{x}, \mathrm{y}, \mathrm{z}, \dot{\mathrm{x}}, \dot{\mathrm{y}}, \dot{\mathrm{z}}) = (\mathrm{x}, -\mathrm{y}, \mathrm{z}, -\dot{\mathrm{x}}, \dot{\mathrm{y}}, -\dot{\mathrm{z}})$$
$$(\mathrm{x}, \mathrm{y}, \mathrm{z}, \dot{\mathrm{x}}, \dot{\mathrm{y}}, \dot{\mathrm{z}}) = (\mathrm{x}, -\mathrm{y}, -\mathrm{z}, -\dot{\mathrm{x}}, \dot{\mathrm{y}}, \dot{\mathrm{z}})$$

When the first condition considered, the xz plane is the plane of symmetry ($\mathrm{syzygy-axis}$). The trajectory crossing the syzygy-axis vertically shows the same motion in opposite side of quadrant. Therefore, if a trajectory crosses the xz plane two times, the trajectory can be closed in the phase space, which is 6 dimensional space composed of position and velocity vectors (see Figure 3.2).

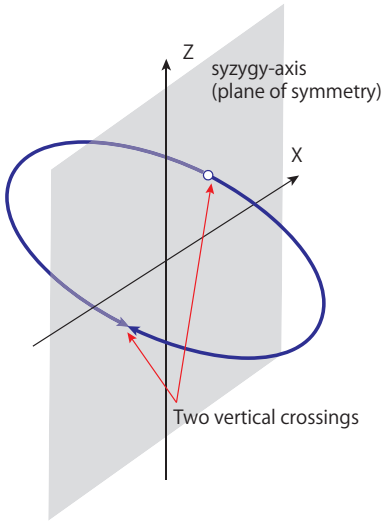

Figure 3.2: Closed Symmetry Orbit

Figure 3.3 shows cloud of Halo orbits around Sun-Earth L2 point in Earth center CR3BP reference coordinate. The blue circle and red cross symbols represent Earth and L2, respectively. The second condition of symmetry indicates that the xy plane can also become the plane of symmetry. Thus, the orbits are classified in two types. The blue curves show the class 1 Halo and the red curves show the class 2 Halo orbits. Class 1 Halo orbits' orbit plane is convex and one of class 2 Halo orbits' is concave and they are symmetry about xy plane. [K.C. 2001]

The presented Halo orbits in Figure 3.3 are ranged from $\mathrm{A_z} = 0$ to 18×10^5 km and the particular orbit has unique properties. Figure 3.4 and Figure 3.5 show respective orbit period and instability, respectively, as an illustration. It is clearly shown that the larger Halo have shorter period and weaker instability and the smaller Halo have longer period and stronger instability in contrast.

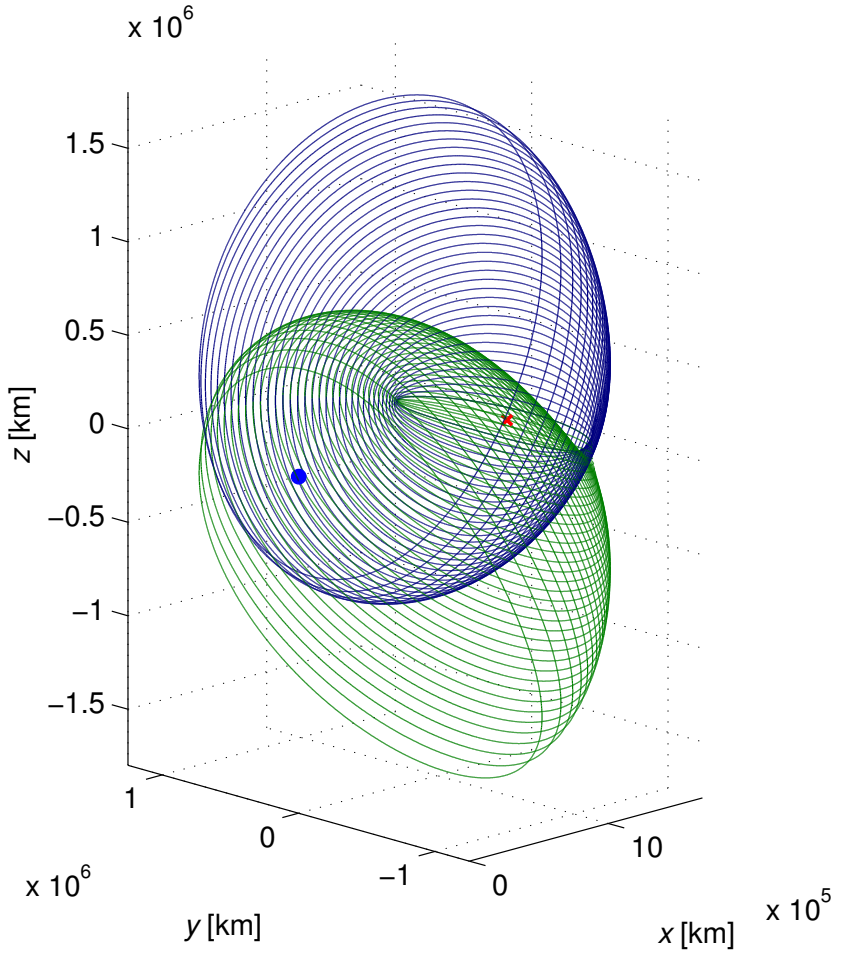

Figure 3.3: Three Dimensional Families of Halo Orbits

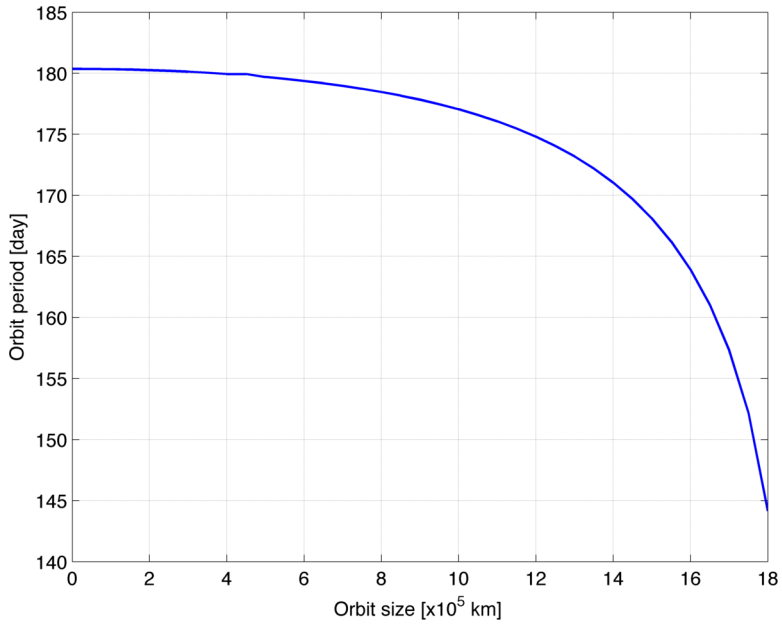

Figure 3.4: Period of Halo Orbits

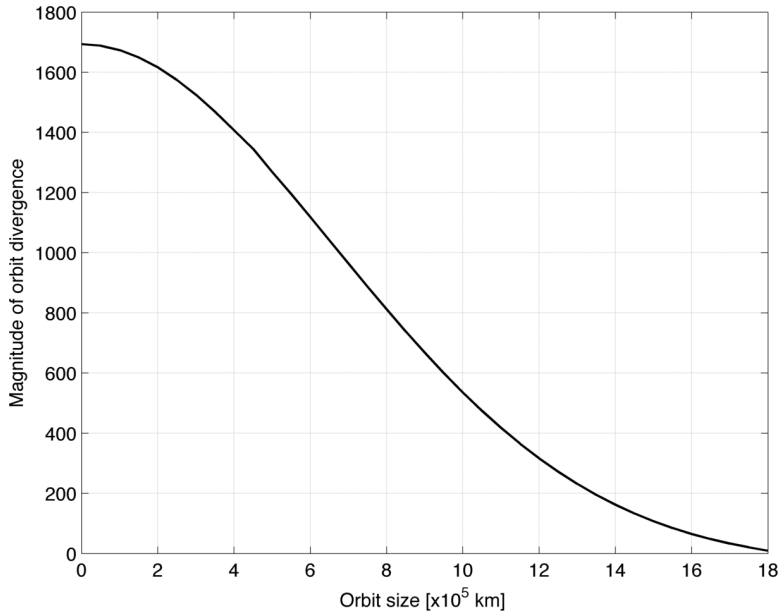

Figure 3.5: Diverging Magnitude of Halo Orbits

CHAPTER 4

Application of Dynamical Systems Theory

Contents

This chapter presents the special maneuver design using Dynamical Systems Theory (DST). The restricted three-body problem is well known as complex dynamical systems and the motion of the particle is often shows the chaotic behavior. Therefore, the application of DST to the trajectory design is exceptionally useful.

At first, principal properties of periodic orbits which obtained from the eigenvalue problem applied to the Monodromy matrix are briefly introduced. In the next, practical use of the obtained properties will be shown for the periodic orbit maintenance.

4.1 Principal Subspace

The State Transition Matrix (STM) is one of the key feature for the trajectory design in this chapter. The STM is the characteristic feature in the DST which can be used to obtain the general solution of linear dynamical systems.

The STM can be obtained by numerical integration of variational equation along the reference trajectory (see A) and it derivers the displacement analysis as long as the displacement stays within linear region of the reference trajectory.

$$\boldsymbol{\delta \mathbf{y}_t} = \boldsymbol{\Phi}(\mathrm{t}_0, \mathrm{t})\boldsymbol{\delta \mathbf{y}_0} \tag{4.1}$$

where $\boldsymbol{\Phi}(\mathrm{t}_0, \mathrm{t})$ is the STM from t_0 until t and $\boldsymbol{\delta \mathbf{y}_0}$ and $\boldsymbol{\delta \mathbf{y}_t}$ are the displacement at t_0 and transferred displacement at t, respectively.

The Monodromy matrix $\mathbf{M}$ is a special matrix of the STM. When the STM is calculated over the periodic motion, the matrix is specially named as Monodromy matrix. Thus;

$$\mathbf{M} = \boldsymbol{\Phi}(0, \mathrm{P}) \tag{4.2}$$

where P is one orbit period.

The Halo orbits shown in Chapter 3 are periodic orbits around the L point in the CR3BP. Therefore, the STM integrated over a whole trajectory of Halo orbit is the Monodromy matrix. When we apply the eigenvalue problem to the Monodromy matrix, the resulting eigenvalues and respective eigenvectors give us principal properties and the directions.

Since the trajectory is designed in three-dimensional space the Monodromy matrix is 6×6 and the 6 eigenvalues are obtained by means of the eigenvalue problem. The calculated eigenvalues are grouped as:

1. Stability pair ; λ_1 and λ_2
2. Rotating pair ; λ_3 and λ_4
3. Neutral pair ; λ_5 and λ_6

The stability pair is a pair of real number eigenvalues. Magnitude of λ_1 is greater than one and λ_2 is reciprocal number of the λ_1. The rotating pair consists of complex conjugate. The neutral pair has real numbers and the magnitude is equal to one because the original matrix is the Monodromy matrix.

Each pair of eigenvalues represents the principal properties and related eigenvectors $\mathbf{e}_\mathrm{i}$ give the principal directions, respectively.

4.2 Relative Motion

In the DST, the invariant manifolds are constructed about the reference trajectory and they represent the linearized motion about the trajectory. [Simanjuntak 2013]

The relationship between eigenvalue and eigenvector is:

$$(\lambda \mathbf{I} - \mathbf{M})\mathbf{e} = \mathbf{0} \tag{4.3}$$

where $\mathbf{I}$ is the identity matrix.

The Monodromy matrix (STM) transfers the displacement about the reference after one period (see 4.1). Hence, a principal subspace is transferred about the reference:

$$\boldsymbol{\delta}\mathbf{y}_{\mathbf{P}}, \mathbf{e} = \lambda \mathbf{e} \tag{4.4}$$

Furthermore, after n-th period, the subspace is transferred as:

$$\boldsymbol{\delta}\mathbf{y}_{\mathbf{nP,e}} = \lambda^{\mathrm{n}} \mathbf{e} \tag{4.5}$$

Therefore, the obtained displacement increase its magnitude if the eigenvalue is greater than one along principal directions. Only the eigenvalue λ_1 has the magnitude greater than one. Consequently, a component of displacement into $\mathbf{e_1}$ stretch the magnitude as much as λ_1.

Note that the rotating subspaces are originally imaginary space. Thus, the eigenvectors are rebuilt to enable the trajectory design in real space:

$$\lambda_{\mathrm{rs}} = \frac{\lambda_3 + \lambda_4}{2} = \cos\theta \tag{4.6}$$

$$\lambda_{\mathrm{rs}} = \frac{\lambda_3 - \lambda_4}{2\mathrm{i}} = \sin\theta \tag{4.7}$$

$$\mathbf{e}_{\mathrm{rs}} = \frac{\mathbf{e}_3 + \mathbf{e}_4}{2} \tag{4.8}$$

$$\mathbf{e}_{\mathrm{rd}} = \frac{\mathbf{e}_3 - \mathbf{e}_4}{2\mathrm{i}} \tag{4.9}$$

The invariant manifolds are, then, designed by giving a small displacements into the principal direction. The stable and unstable manifolds provided in Figure 1.2 are illustrating diverging and converging motions about the nominal trajectory. The other manifolds stay close to the reference. The rotating manifolds about Halo reference are called Quasi-Halo orbits and the neutral manifolds are named as along and cross track trajectories.

4.3 Orbit Maintenance Maneuver Design

4.3.1 Scheme

The Lagrangian points missions especially around collinear points requires precise orbit design since the orbits are highly unstable. In contrast, for the actual mission operation, it is not necessary that a spacecraft flights exactly on the reference orbit as long as it is not deviated from the orbit. Therefore, the reasonable correction maneuver can be designed to reduce the orbit maintenance maneuver. [Ikenaga 2011]

Figures 4.1 illustrates the growing displacement. The black arrows show the principal directions matched with eigenvectors of the Monodromy matrix and read solid arrow shows the displacement vector with respect to reference orbit shown in a blue face circle.

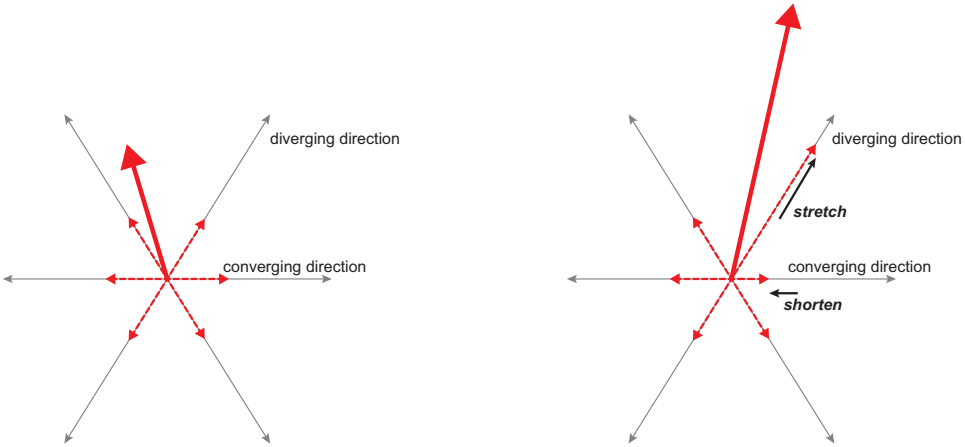

Figure 4.1: Growing Displacement from Reference

The diverging eigenvector is only the error growing direction for the periodic orbit since the other eigenvalue magnitude is smaller or equal to one. Thus, eliminating the diverging component from the displacement the displacement will not increase the magnitude (see Figure 4.2).

4.3.2 Error Suppressing Orbit Maintenance

The error suppressing method is a reasonable correction approach for the periodic orbit maintenance. The relative motions as refer to above show that only one subspace stretches the displacement (error) about the nominal trajectory. Hence, it is possible to maintain the flight trajectory nearby the nominal trajectory by means of suppressing the error by removal of di-

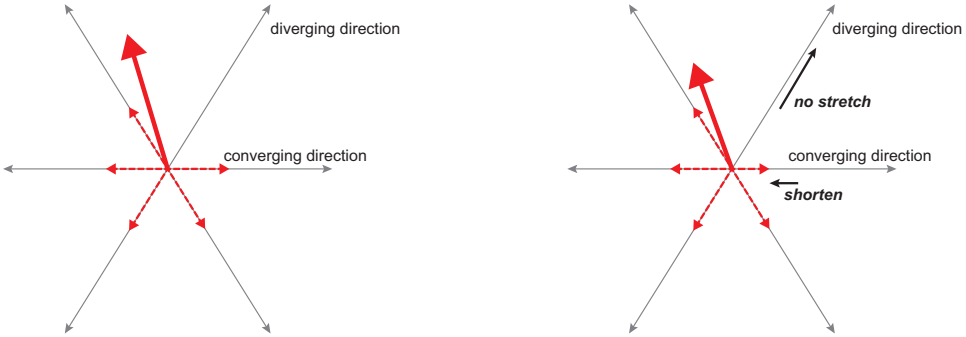

Figure 4.2: Non-Growing Displacement after Maneuver

verging component. The eigenvector directs 6-dimensional subspace and, therefore, the maneuver design may not be the simple.

First the given error is distributed onto each direction as:

$$\boldsymbol{\delta y_0} = \begin{bmatrix} \boldsymbol{\delta r_0} \\ \boldsymbol{\delta v_0} \end{bmatrix} = [\mathbf{e}_\mathrm{d}, \mathbf{e}_\mathrm{c}, \mathbf{e}_\mathrm{rs}, \mathbf{e}_\mathrm{rd}, \mathbf{e}_\mathrm{at}, \mathbf{e}_\mathrm{ct}][\mathrm{c}_\mathrm{d}^*, \mathrm{c}_\mathrm{c}^*, \mathrm{c}_\mathrm{rs}^*, \mathrm{c}_\mathrm{rd}^*, \mathrm{c}_\mathrm{at}^*, \mathrm{c}_\mathrm{ct}^*]^\mathrm{T} \quad (4.10)$$

where c_i^* is the coefficient and the subscripts d, c, at and ct represent diverging, converging, along track and cross track directions, respectively.

The eigenvector $\mathbf{e}_\mathrm{d}$ is defined as the error stretching direction. Thus, when c_1^* is zero, the displacement will not be grown.

The Monodromy matrix is propagated by linearized equation and, therefore, the matrix does not transfer the state exactly when the displacement becomes large (higher order term start disturbing).

Next, adding an impulsive velocity correction $\boldsymbol{\Delta v}$ to cancel the component of diverging direction ($\mathrm{c}_\mathrm{d}\mathbf{e}_\mathrm{d}$) from the given error as:

$$\begin{bmatrix} \boldsymbol{\delta r_0} \\ \boldsymbol{\delta v_0} \end{bmatrix} + \begin{bmatrix} \mathbf{0} \\ \boldsymbol{\Delta v} \end{bmatrix} = [\mathbf{e}_\mathrm{d}, \mathbf{e}_\mathrm{c}, \mathbf{e}_\mathrm{rs}, \mathbf{e}_\mathrm{rd}, \mathbf{e}_\mathrm{at}, \mathbf{e}_\mathrm{ct}][0, \mathrm{c}_\mathrm{c}, \mathrm{c}_\mathrm{rs}, \mathrm{c}_\mathrm{rd}, \mathrm{c}_\mathrm{at}, \mathrm{c}_\mathrm{ct}]^\mathrm{T} \quad (4.11)$$

Now, we construct the matrix $\mathbf{X}$ consists of eigenvectors and divide the matrix into 4 segments. The each matrix X_i has 3×3 elements.

$$[\mathbf{e}_\mathrm{d}, \mathbf{e}_\mathrm{c}, \mathbf{e}_\mathrm{rs}, \mathbf{e}_\mathrm{rd}, \mathbf{e}_\mathrm{at}, \mathbf{e}_\mathrm{ct}] = \mathbf{X} = \begin{bmatrix} \mathrm{X}_1 & \mathrm{X}_2 \\ \mathrm{X}_3 & \mathrm{X}_4 \end{bmatrix} \quad (4.12)$$

The position displacement and velocity displacement with velocity correction are then calculated by:

$$\boldsymbol{\delta \mathbf{r_0}} = \mathrm{X}_1 \begin{bmatrix} 0 \\ \mathrm{c_c} \\ \mathrm{c_{rs}} \end{bmatrix} + \mathrm{X}_2 \begin{bmatrix} \mathrm{c_{rd}} \\ \mathrm{c_{at}} \\ \mathrm{c_{ct}} \end{bmatrix} \tag{4.13}$$

$$\boldsymbol{\delta \mathbf{v_0}} + \boldsymbol{\Delta \mathbf{v}} = \mathrm{X}_3 \begin{bmatrix} 0 \\ \mathrm{c_c} \\ \mathrm{c_{rs}} \end{bmatrix} + \mathrm{X}_4 \begin{bmatrix} \mathrm{c_{rd}} \\ \mathrm{c_{at}} \\ \mathrm{c_{ct}} \end{bmatrix} \tag{4.14}$$

From Eq. 4.13, the coefficients $\mathrm{c_{rd}}$ to $\mathrm{c_{ct}}$ are expressed by $\mathrm{e_c}$ and $\mathrm{e_{rs}}$ as:

$$\begin{bmatrix} \mathrm{c_{rd}} \\ \mathrm{c_{at}} \\ \mathrm{c_{ct}} \end{bmatrix} = \mathrm{X}_2^{-1} \boldsymbol{\delta \mathbf{r_0}} - \mathrm{X}_2^{-1} \mathrm{X}_1 \begin{bmatrix} 0 \\ \mathrm{c_c} \\ \mathrm{c_{rs}} \end{bmatrix} \tag{4.15}$$

Substituting Eq. 4.15 into Eq. 4.14, we get the required velocity correction:

$$\boldsymbol{\Delta \mathbf{v}} = \mathbf{A} \begin{bmatrix} 0 \\ \mathrm{c_c} \\ \mathrm{c_{rs}} \end{bmatrix} + \mathbf{B} \tag{4.16}$$

where $\mathbf{A}$ is a 3×3 matrix

$$\mathbf{A} = (\mathrm{X}_3 - \mathrm{X}_4(\mathrm{X}_2^{-1}\mathrm{X}_1)) \tag{4.17}$$

and $\mathbf{B}$ is a three elements column vector

$$\mathbf{B} = \mathrm{X}_4(\mathrm{X}_2^{-1}\boldsymbol{\delta \mathbf{r}}) - \boldsymbol{\delta \mathbf{v}} \tag{4.18}$$

4.3.3 Linear Algebra Approach Finding Minimum Solution

It is observed in Eq. 4.16 that the calculation of required $\boldsymbol{\Delta \mathbf{v}}$ has two degree of freedom with design parameters $\mathrm{c_c}$ and $\mathrm{c_{rs}}$.

When the coefficients $\mathrm{c_c}$ and $\mathrm{c_{rs}}$ are selected appropriately the magnitude of required $\Delta \mathrm{v}$ becomes minimum. The following explains the solution of minimum $\Delta \mathrm{v}$ finding by using the algebra approach.

From Eq. 4.16 the sum square of $\Delta \mathrm{v}$ is expressed in terms of $\mathrm{c_c}$ and $\mathrm{c_{rs}}$. These variables are replaced to x and y

$$|\Delta \mathrm{v}|^2 = \mathrm{s}^2\mathrm{x}^2 + \mathrm{t}^2\mathrm{y}^2 + \mathrm{u}^2 + 2\mathrm{kxy} + 2\mathrm{lx} + 2\mathrm{my} \tag{4.19}$$

where s, t, u, k, l and m are factors.

While the square of the $\Delta \mathrm{v}$ is a quadric equation with two variables x and y, therefore it can be factorized as:

$$|\Delta \mathrm{v}|^2 = (\alpha \mathrm{x} + \beta \mathrm{y} + \gamma)^2 + (\zeta \mathrm{y} + \xi)^2 + \eta^2 \tag{4.20}$$

This implies that $\Delta \mathrm{v}$ takes minimum value η when x and y satisfy;

$$\mathrm{x} = -(\frac{\beta\xi}{\zeta} + \gamma)/\alpha \tag{4.21}$$

and

$$\mathrm{y} = -\frac{\xi}{\zeta} \tag{4.22}$$

Equating Eq. 4.19 and Eq. 4.20, x and y can be calculated in strait forward way.

4.3.4 Relation of Minimum $\Delta \mathrm{v}$ and Initial Displacement

The initial displacement is distributed onto 6 principal directions as Eq. **??**. Thus, position and velocity displacements are expressed in terms of matrix $\mathrm{X_i}$ similar to Eqs. 4.13 and 4.14:

$$\boldsymbol{\delta \mathbf{r_0}} = \mathrm{X}_1 \begin{bmatrix} \mathrm{c}_{\mathrm{d}}^* \\ \mathrm{c}_{\mathrm{c}}^* \\ \mathrm{c}_{\mathrm{rs}}^* \end{bmatrix} + \mathrm{X}_2 \begin{bmatrix} \mathrm{c}_{\mathrm{rd}}^* \\ \mathrm{c}_{\mathrm{at}}^* \\ \mathrm{c}_{\mathrm{ct}}^* \end{bmatrix} \tag{4.23}$$

$$\boldsymbol{\delta \mathbf{v_0}} = \mathrm{X}_3 \begin{bmatrix} \mathrm{c}_{\mathrm{d}}^* \\ \mathrm{c}_{\mathrm{c}}^* \\ \mathrm{c}_{\mathrm{rs}}^* \end{bmatrix} + \mathrm{X}_4 \begin{bmatrix} \mathrm{c}_{\mathrm{rd}}^* \\ \mathrm{c}_{\mathrm{at}}^* \\ \mathrm{c}_{\mathrm{ct}}^* \end{bmatrix} \tag{4.24}$$

Substituting Eqs. 4.23 and 4.24 into Eq. 4.18 the vector B is shown as:

$$\begin{aligned}\mathbf{B} &= \mathrm{X_4}[\mathrm{X_2^{-1}}(\mathrm{X_1}\begin{bmatrix} \mathrm{c_d^*} \\ \mathrm{c_c^*} \\ \mathrm{c_{rs}^*} \end{bmatrix} + \mathrm{X_2}\begin{bmatrix} \mathrm{c_{rd}^*} \\ \mathrm{c_{at}^*} \\ \mathrm{c_{ct}^*} \end{bmatrix})] - (\mathrm{X_3}\begin{bmatrix} \mathrm{c_d^*} \\ \mathrm{c_c^*} \\ \mathrm{c_{rs}^*} \end{bmatrix} + \mathrm{X_4}\begin{bmatrix} \mathrm{c_{rd}^*} \\ \mathrm{c_{at}^*} \\ \mathrm{c_{ct}^*} \end{bmatrix}) \\ &= [\mathrm{X_4}(\mathrm{X_2^{-1}X_1}) - \mathrm{X_3}]\begin{bmatrix} \mathrm{c_d^*} \\ \mathrm{c_c^*} \\ \mathrm{c_{rs}^*} \end{bmatrix} \qquad (4.25) \\ &= -\mathbf{A}\begin{bmatrix} \mathrm{c_d^*} \\ \mathrm{c_c^*} \\ \mathrm{c_{rs}^*} \end{bmatrix}\end{aligned}$$

Finally, we get the $\Delta \mathrm{v}$ as:

$$\mathbf{\Delta v} = \mathbf{A}\begin{bmatrix} -\mathrm{c_d^*} \\ \mathrm{c_c} - \mathrm{c_c^*} \\ \mathrm{c_{rs}} - \mathrm{c_{rs}^*} \end{bmatrix} \qquad (4.26)$$

Likewise the procedure provided in previous section, sum square of the $\Delta \mathrm{v}$ is considered and it is expressed as:

$$|\Delta \mathrm{v}|^2 = \mathrm{S^2 c_c'^2} + \mathrm{T^2 c_{rs}'^2} + \mathrm{U^2 c_d^*} + 2\mathrm{K c_c' c_{rs}'} + 2\mathrm{L c_d^* c_c'} + 2\mathrm{M c_d^* c_{rs}'} \qquad (4.27)$$

where $\mathrm{c_c'}$ and $\mathrm{c_{rs}'}$ represent $\mathrm{c_c} - \mathrm{c_c}^*$ and $\mathrm{c_{rs}} - \mathrm{c_{rs}}^*$, respectively.

The equation can be completed squared similar to Eq.4.20 seeing that the parameters are again two coefficients $\mathrm{c_c}$ and $\mathrm{c_{rs}}$. Equating the factors in Eqs. 4.20 and 4.27, the minimum value could become;

$$\Delta \mathrm{v} = \sqrt{\mathrm{u^2} + (\frac{\mathrm{l}}{\alpha})^2 - (\mathrm{m} - \frac{\beta \mathrm{l}}{\alpha})^2}\ \mathrm{c_d^*} \qquad (4.28)$$

Therefore, by selecting $\mathrm{c_c}$ and $\mathrm{c_{rs}}$ properly, only the minimum solution of $\Delta \mathrm{v}$ is calculated from the elements of given matrix $\mathbf{A}$ and $\mathrm{c_d^*}$. Consequently, the magnitude of minimum $\Delta \mathrm{v}$ is proportional to the coefficient of the diverging eigenvector in given error. The other components (coefficients) do not affect on the minimum solution.

4.3.5 Application to Halo Orbit

The CR3BP is the perfectly symmetry and autonomous model of the restricted three-body problem. Halo orbits are found around the collinear

equilibrium points in various shape in the CR3BP. The practical use of this method has been shown by Nakamiya [Nakamiya, 2012] by controlling the spacecraft unloading maneuver direction assuming an actual spacecraft SPICA's configuration.

The Halo orbits have their own properties depending on the shape (see Figures 3.4 and 3.5). The reference orbit can be chosen arbitrary because all the Halo orbits are periodic. For an demonstration, a Halo orbit whose shape is $4.0 \times 10^5 \mathrm{km}(\mathrm{A_z})$ selected (Figure 4.3).

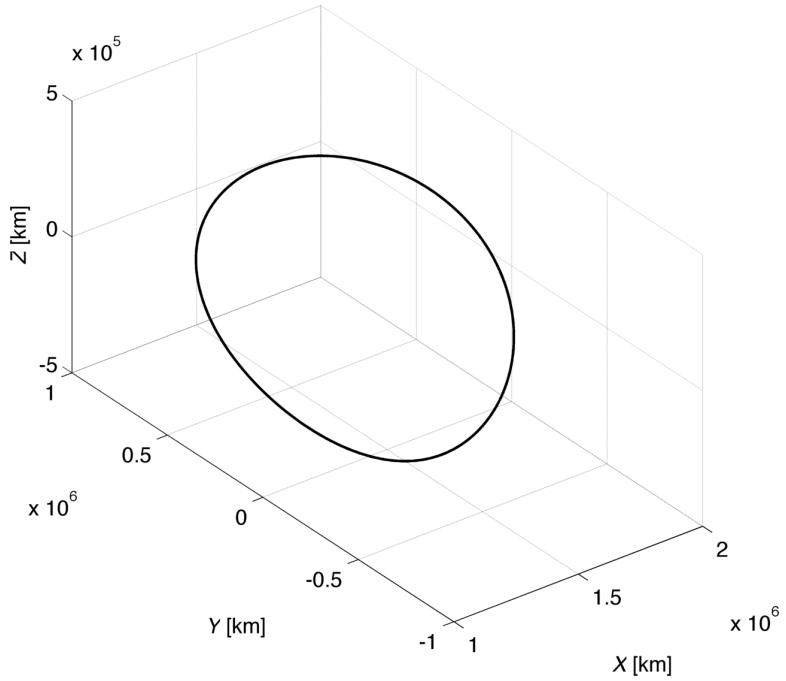

Figure 4.3: Reference Halo Orbit in Earth Center Rotating Reference

Table 4.1 summarizes the orbit properties of the reference Halo orbit. The $\mathbf{e}_6$ is identical to along track direction $\mathbf{e}_5$. The cross track direction is modified from the original eigenvector $\mathbf{e}_6$ to have cross track property [Triwanto 2012].

4.3.5.1 Artificial Error

The state displacements is assumed and given at the initial condition $\boldsymbol{\delta}\mathbf{r_0}$ and $\boldsymbol{\delta}\mathbf{v_0}$. The initial displacement is identically distributed along each six axis direction namely $\mathbf{x}, \mathbf{y}, \mathbf{z}, \dot{\mathbf{x}}, \dot{\mathbf{y}}, \dot{\mathbf{z}}$ and the magnitude of the displacement is as large as 10 km in position error (along $\mathbf{x}, \mathbf{y}, \mathbf{z}$ axes) and 1 mm/s in velocity error (along $\dot{\mathbf{x}}, \dot{\mathbf{y}}, \dot{\mathbf{z}}$ axes). The coefficients for each direction are shown in Table 4.2

Table 4.1: Reference Halo Orbit Properties

Orbit Period	
179.9 days	
Principal Properties	
Definition	Direction
Diverging	[-0.376,0.121,-0.023,-0.816,0.392,-0.153]
Converging	[-0.376,-0.121,-0.023,0.816,0.392,0.153]
Rotating (rs)	[0.0,0.474,0.0,0.481,0.0,-0.343]
Rotating (rd)	[0.117,0.0,-0.433,0.0,-0.475,0.0]
Along Track	[0.0,-0.639,0.0,-0.574,0.0,-0.511]
Cross Track	[0.059,0.0,-0.836,0.0,0.546,0.0]

Table 4.2: Required Correction Maneuver

Error direction	Coefficients vector $[\mathrm{c_d}, \mathrm{c_c}, \mathrm{c_{rs}}, \mathrm{c_{rd}}, \mathrm{c_{at}}, \mathrm{c_{ct}}] \times 10^{-8}$]
x	[-9.94, -9.94, 0.0, -9.79, 0.0, 5.75]
y	[3.40, -3.40, 5.06, 0.0, -5.43, 0.0]
z	[-1.44, -1.44, 0.0, -7.18, 0.0, -4.18]
$\dot{\mathrm{x}}$	[-1.78, 1.78, 1.23, 0.0, 0.24, 0.0]
$\dot{\mathrm{y}}$	[-0.57, -0.57, 0.0, -4.99, 0.0, 2.62]
$\dot{\mathrm{z}}$	[-0.13, 0.13, -4.56, 0.0, -3.43, 0.0]

4.3.5.2 Correction $\Delta \mathrm{v}$

The required correction $\Delta \mathrm{v}$ are calculated from constructed artificial errors and obtained Monodromy matrix substituting in Eq. 4.16 and searched the minimum solution by Eq. 4.20 - 4.22. Table 4.3 show the results for each direction of error. Comparing with the resulting maneuver magnitude and diverging coefficient (see also in Figure 4.4), it is in a particular relationship as predicted in Eq. 4.28. For a sample case, we give a random displacement such as $[8.14, 9.06, 1.27, 9.13, 6.32, 9.75] \times 10^8$, which has -1.37×10^7 of the diverging coefficient. For the error, required maneuver comes 7.33×10^3 km and the magnitude is matched with the proportion of the diverging coefficients and maneuver magnitude.

In summary, the suppression maneuver that cancel the diverging subspace in state displacement. Therefore, the propagated trajectory after

Table 4.3: Coefficients of Given Error into Principal Directions

Error direction	Δv	
	Direction [x, y, z] [$\times 10^{-3}$ m/s]	Magnitude [$\times 10^{-3}$ m/s]
x	[-5.04, -1.62, -0.37]	5.31
y	[1.72, 0.55, 0.13]	1.82
z	[-0.73, -0.23, -0.05]	0.77
$\dot{x}$	[-0.92, -0.28, -0.07]	0.95
$\dot{y}$	[-0.29, -0.09, -0.02]	0.30
$\dot{z}$	[-0.07, -0.02, -0.01]	0.07

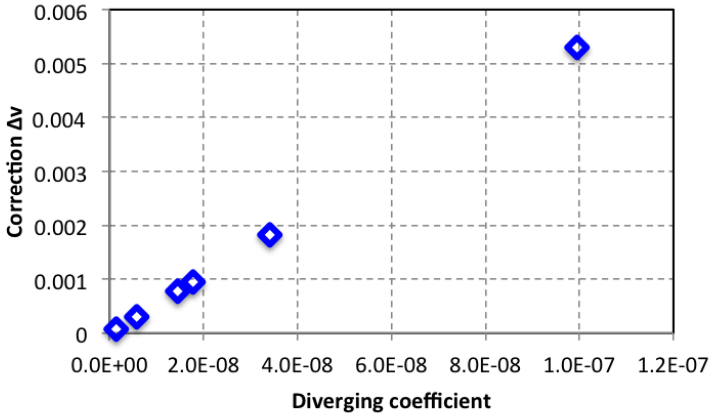

Figure 4.4: Relationship between Diverging Coefficient and Maneuver

the suppression maneuver stay close to the nominal trajectory and will not be deviated.

CHAPTER 5

Periodic Orbits in ER3BP

Contents

5.1 Definition of Periodic Orbits

This chapter presents the periodic orbit design method in ER3BP around the Sun-Earth L2 point. The purpose is to find the Halo orbit like periodic orbit by continuous orbit propagation. The "Halo orbit like" indicates the orbit is elliptic around the corresponding L point.

In the ER3BP, periodic orbits can be designed when the two following sufficient conditions are satisfied [1920 Moulton]. Moulton investigated the planer periodic orbits and Campagnola showed three-dimensional periodic orbits. [2008 Campagnola]

- Two vertically crossing at the symmetry plane
- The symmetry plane crossings happen at $\mathrm{f} = 0$ or π

The first condition is same as the sufficient condition for Halo orbits. The second condition derives from the time dependency of the model. The ER3BP could be the symmetry model only with respect to apse line ($\mathrm{f} = \pi - 2\pi$).

Chapter 3 shows the Halo orbits designed in CR3BP. The Halo orbits are known as pure periodic orbits around collinear Lagrange points which come back at the same position and velocity after arbitrary periods depending on the orbit size. However, the ER3BP is not autonomous model since the motion in the ER3BP is depending on the epoch of the primaries.

Therefore, it is not possible to design periodic orbits like Halo orbits in the ER3BP only by satisfying the first sufficient condition. To satisfy the second sufficient condition, it is necessary that the orbit period is in ratio of integer with the primaries orbit period

$$\mathrm{P} = \frac{\mathrm{b}}{\mathrm{a}}\pi \tag{5.1}$$

5.2 Short Period Orbits

5.2.1 Statement

The definition of the short period orbits is that the orbit is designed in one continuous propagation to satisfy the sufficient conditions. Figure 3.4 shows the period of Halo orbit is almost half of the primaries period at most. Therefore, the period should be selected shorter than π at most .

The long period of Halo orbits have large orbit divergence and required number of revolution becomes large. When the accumulated diverging magnitude exceeds 10^6 over the propagation, the numerical differential correction does not work properly. Therefore, for such sensitive orbits, it is difficult to complete the orbit in a continuous orbit propagation.

There are two types of periodic orbits. Figure 5.1 illustrates the different type of periodic orbits geometry expanding nearby the initial condition. Thick solid arrow represent the initial and terminal orbit and eased lines show the intermediate trajectories.

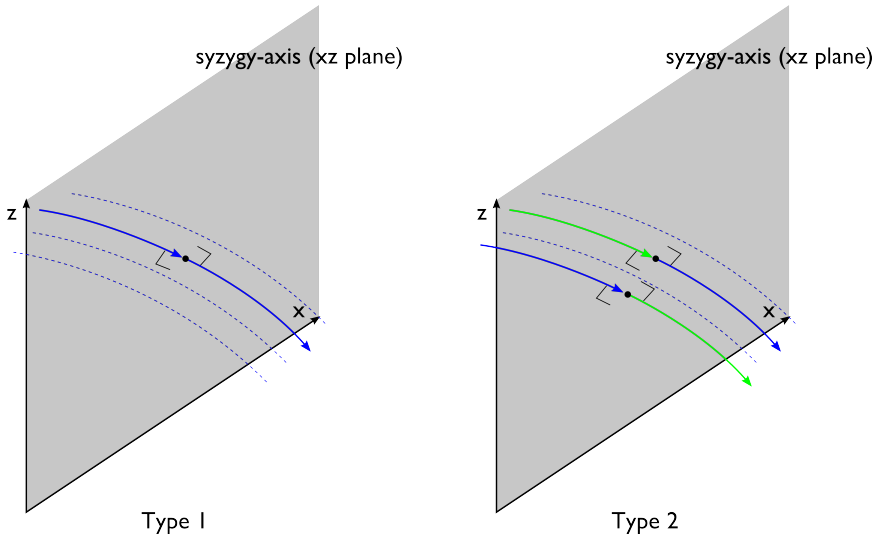

Figure 5.1: Type 1 & Type 2 Periodic Orbit

As shown in Figure 5.1 Type 1 orbits cross xz-plane vertically twice, starting the plane vertically and arriving at the same position vertically after a specific period. Whereas Type 2 orbits cross xz-plane vertically three times at initial, center and terminal of the orbit.

After the specific number of revolution as same as number of a in Eq. 5.1, the time T becomes:

$$\mathrm{T} = \mathrm{P} \times \mathrm{a} = \mathrm{b}\pi \tag{5.2}$$

Depending on the number of b numerator of Eq. 5.1 the periodic orbit type changes whether Type 1 or Type 2.

When T is even multiple of π, the terminal epoch comes back at the initial epoch after a-th revolution. In contrast, when T is odd multiple of π, the terminal epoch is 180° opposite to the initial epoch after a-th revolution.

The second sufficient condition shows two vertical crossings at $\mathrm{f} = 0$ and π is enough for the periodic orbit design but in that case (Type 2), in order to reproduce the state completely, the orbit requires another a-th revolutions represented in green arrow in Figure 5.1 ($2\mathrm{a}$ revolutions in total).

Additionally, since the Type 1 orbits starts and comes back at the same location on xz-plane they have two classes as $\mathrm{f} : 0 - 0$ and $\mathrm{f} : \pi - \pi$.

5.2.2 Design Examples

Again the Halo orbits are no more exist in ER3BP. However, if the eccentricity of the primaries is zero, the eccentric term of the ER3BP equations of motion are cancelled (see Eqs. 2.44-2.45) and they are concluded as the CR3BP equations of motion. It means that motion in the ER3BP with very small eccentricity can be approximated by the CR3BP. Thus, the initial condition of the Halo orbits are still useful for periodic orbit design in ER3BP initial estimation.

As an illustration, two Halo orbits, whose period are $\frac{1}{2}\pi$ and $\frac{2}{3}\pi$, are selected as initial approximations (see Figure 5.2 and 5.3). The left and right side of the figure is the in plane and out plane projections of the orbit and the black circle shows the initial condition. Judged from the numerator of the period, $\mathrm{P} = \frac{1}{2}\pi$ Halo is going to be the type 2 periodic orbit and $\mathrm{P} = \frac{2}{3}\pi$ Halo will be the type 1 periodic orbit.

Table 5.1 presents the numerical value of initial conditions of the estimated Halo orbits. Since the orbit starts on the xz-plane vertically, the initial position along y-axis and velocity along x and z axes are fixed parameter to zero.

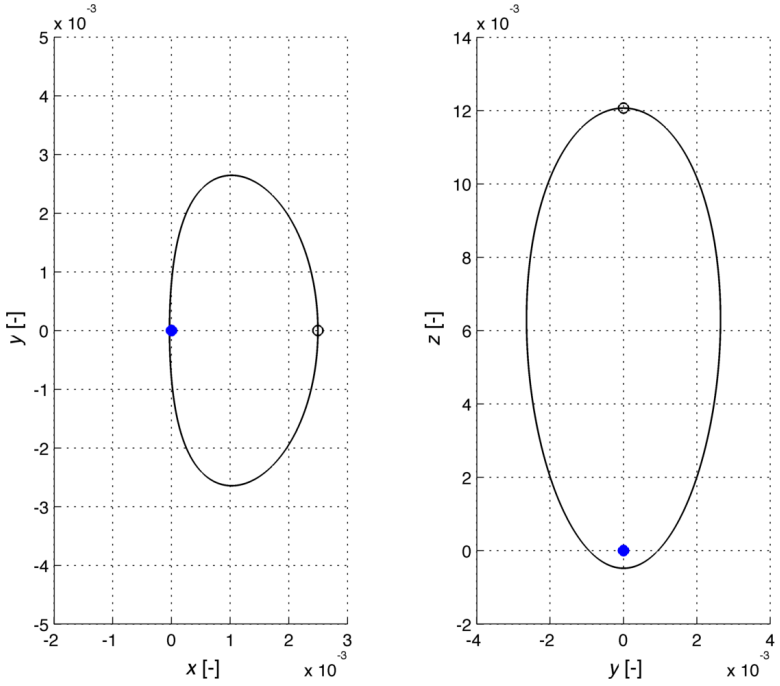

Figure 5.2: Halo Orbit in CR3BP ($\mathrm{P} = \frac{1}{2}\pi$)

Table 5.1: Initial Condition of Halo Orbit

P	x_0	z_0	$\dot{\mathrm{y}}_0$
$\pi/2$	1.00249	0.01206	-0.00639
$2\pi/3$	1.00557	0.01234	-0.01239

It is important that even relatively small eccentricity like Sun-Earth system ($\mathrm{e} = 0.0167$) can be a strong anomaly source of the orbit deviation. Thus, first the initial estimated initial condition is not be used directly for the orbit design and very small eccentricity like $\mathrm{e} = 10^{-6}$ is used for the start. The continuation method is taken instead of designing orbit directly in the actual eccentricity.

Starting the initially estimated conditions presented in previous section the periodic orbits have been designed in ER3BP. Figures 5.4 - 5.6 shows the obtained initial conditions of the x_0, z_0 and $\dot{\mathrm{y}}_0$ by means of the continuation method to find the periodic solution in terms of the eccentricity. For each figure, both horizontal and vertical axes are shown in log scale and the non-filled symbols, what representing the difference value of initial conditions of the periodic orbits from the estimated initial conditions,

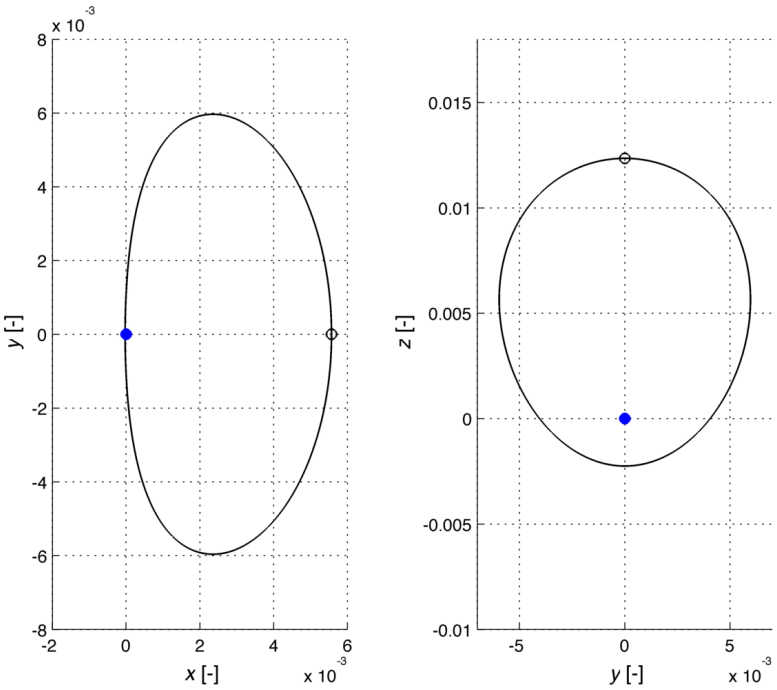

Figure 5.3: Halo Orbit in CR3BP ($\mathrm{P} = \frac{2}{3}\pi$)

are plotted on the strait line. Therefore, the periodic orbit designed in the small eccentricity model can simply extrapolates the other periodic orbits in arbitrary eccentricity model.

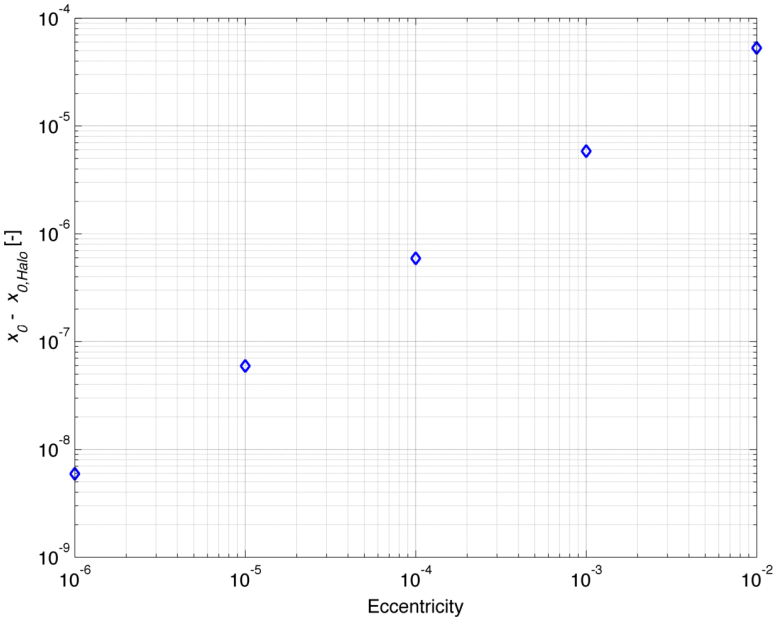

Figure 5.4: Variation of the Initial Position x_0

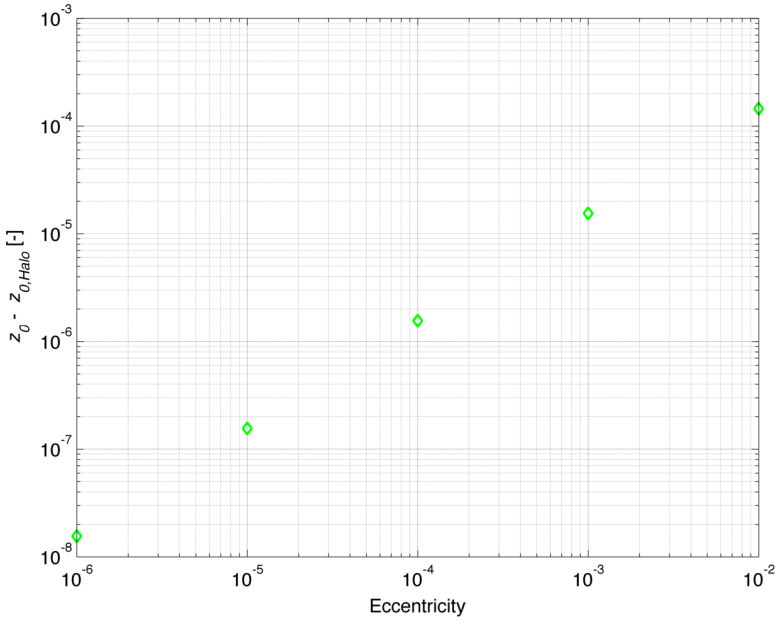

Figure 5.5: Variation of the Initial Position z_0

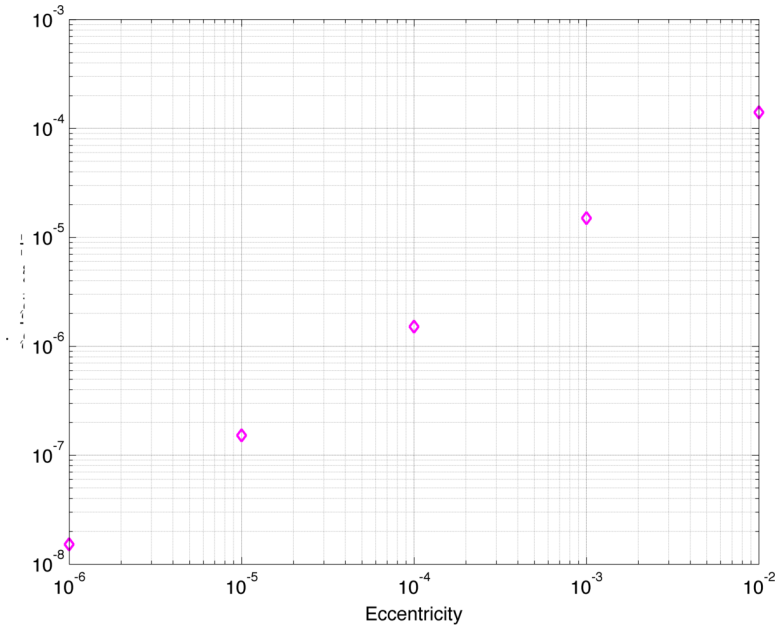

Figure 5.6: Variation of the Initial Velocity $\dot{y}_0$

Finally, designed periodic orbit in $e = 0.01$ ER3BP, which is slightly smaller eccentricity model than actual eccentricity of the Sun-Earth system, are provided in Figure 5.7 and 5.8. The periodic orbits are classified by the resonant revolution number with primaries which can be given by the orbit period divided by primaries orbit period 2π.

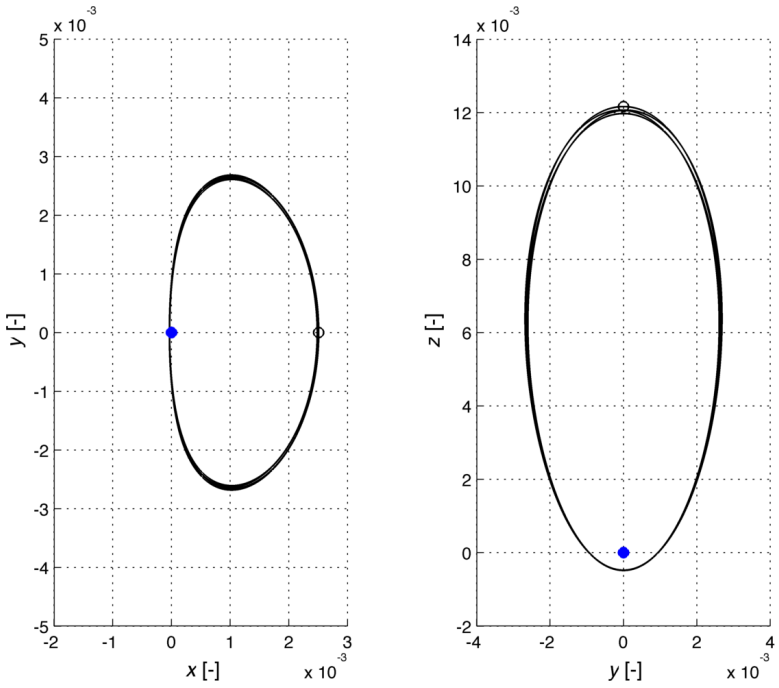

Figure 5.7: 1:4 Periodic Orbit

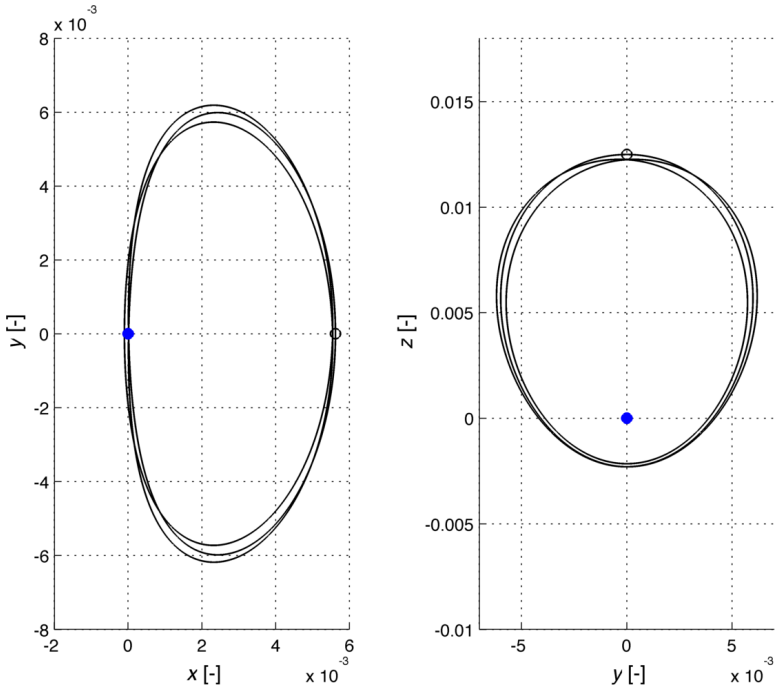

Figure 5.8: 1:3 Periodic Orbit

In the end, the initial estimation is given by the initial condition of the CR3BP Halo orbit. Therefore, the orbit allowable region is defined once

the orbit period is given. Furthermore, the designed short period orbits seem to be almost Earth orbits instead of around the L2 point orbit. Hence, the orbit design can be completed by straight forward way but it is not practical for the L point mission orbit. On the other hand, the properties of the designed periodic orbits are still useful to design other periodic orbits.

CHAPTER 6

Long Period Orbits Construction

Contents

6.1 Problem Statement

This chapter investigates the special technic to design periodic orbits in ER3BP when the orbit period becomes longer. Chapter 5 presents the periodic orbit design in ER3BP especially for the shorter period of orbits and two type of periodic example orbits are shown. Those orbits can be designed directly by numerical differential correction with a continuous trajectory because the orbit has smaller magnitude of divergence and shorter propagation duration required. However, the shorter period orbits exist around secondary body, *e.g.* Earth, and they are not suitable for the L point missions. In order to get orbit around L pint, the longer period of orbit is essential.

The Halo orbits are found near L2 when the period of orbit becomes longer but they have strong diverging magnitude (see Figure 3.5). The periodic orbits in the ER3BP needs integer number of revolution depending on the orbit period to satisfy the sufficient conditions. In that case, the diverging magnitude during one orbit period will be multiplied in each revolution. Consequently, the longer period of orbit makes the orbit design problem by numerical differential correction difficult in the ER3BP.

Figure 6.1 gives a Halo orbit in CR3BP as an illustration of longer orbit period. The period of the Halo is $8/9\pi$, a bit longer than provided $\pi/2$ and $2\pi/3$, and the diverging magnitude over a period is approximately 54.5 which is obtained by maximum eigenvalue of the Monodromy matrix. in addition the number is bigger than previously presented orbits which are around 3 to 5.

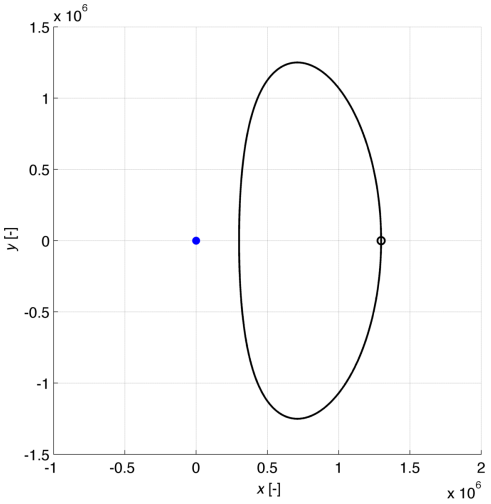

(a) In plane projection

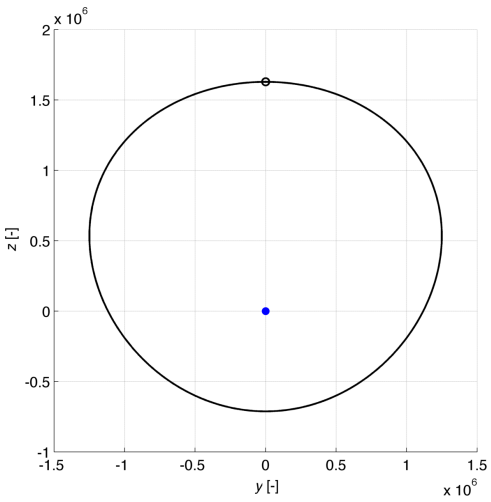

(b) Out plane projection

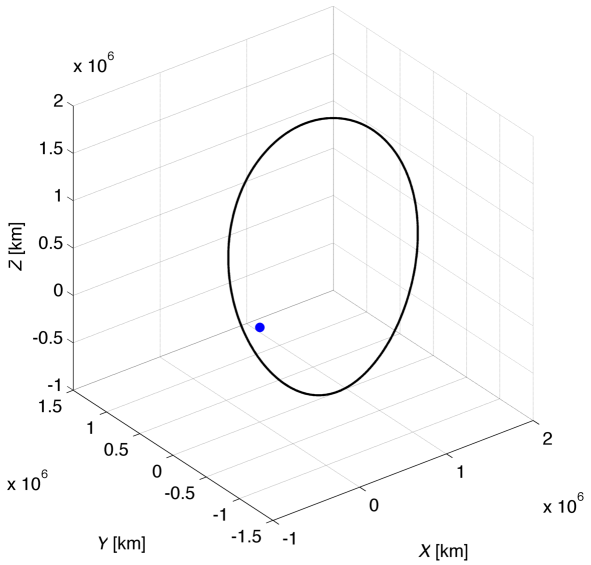

(c) Orbit in 3-dimension

Figure 6.1: Halo Orbit in CR3BP $\mathrm{P} = \frac{8}{9}\pi$

Table 6.1 summarizes the orbit properties. D.M. represents diverging magnitude of the orbit with a revolution and with full revolution. The prop-

erty proves that the direct orbit design method is not possible for given orbit because the diverging magnitude over the full length trajectory will be much bigger than 10^7.

Table 6.1: Orbit Properties of Halo Orbit ($\mathrm{P} = \frac{8}{9}\pi$)

P	x_0	z_0	$\dot{y}_0$	D.M.
$8\pi/9$	1.00867	0.01089	-0.01514	54.5(one), 4.23×10^{15} (full)

The given period of orbit needs 9-revolution to construct the orbit closing in ER3BP following description in chapter 5 and the diverging magnitude is resulting in roughly 4×10^{15}. The differential correction modify the initial condition by obtained error at the final state. Hence, to converge the iteration, within 1km of position and 1mm/s of velocity discrepancy, the resulting diverging magnitude has maximum permitted range (up to 10^7 in this study). Thus, apparently the provided orbit exceed the permitted orbit divergence.

6.2 Design Strategy

This study proposes three processes to find long period orbits. Figure 6.2 illustrates the design process of long period orbits compared with the short period orbits. The short and long period orbits uses the initial approximation given by the Halo orbits. The short period orbits are then found the periodic solution in ER3BP by performing numerical differential correction (DC). The long period orbits may not be taken the same process because of the strong orbit divergence. Thus, it needs the special designing technic. First, the orbit is decided into several segments: $\mathrm{Step1}$. Next, the periodic orbit with control maneuvers is designed by patching the divided orbits: $\mathrm{Step2}$. Finally, the required control maneuvers are neglected by giving adequate connection condition: $\mathrm{Step3}$.

Step 1: Orbit Separation

The whole periodic orbit is separated into several segments and orbit in each segment is linearized. The number of revolution included in each segment is defined depending on the orbit diverging magnitude. The accumulated total diverging magnitude is maintained smaller than 10^7 to hold the stable convergence. For the given initial estimated orbit, the 9-revolution of orbit is divided into three segments each segment has 3-revolution. The orbit in each segment is designed by numerical differential correction to

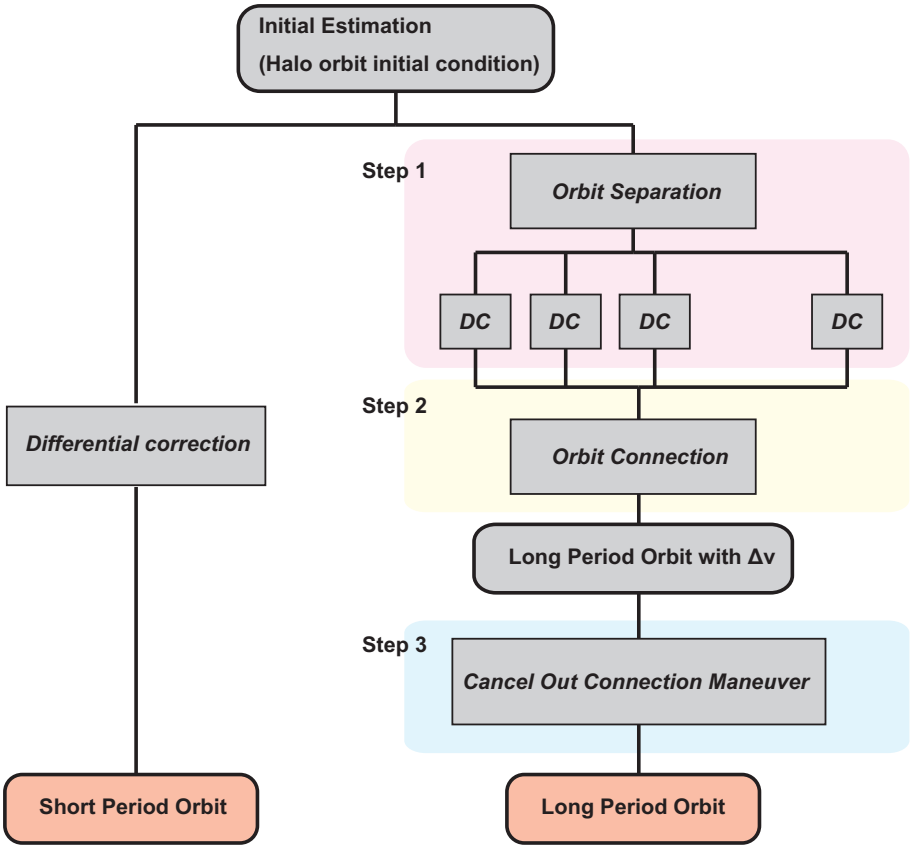

Figure 6.2: Illustration of Periodic Orbit Design Process

make the trajectory end match with the target location. More longer orbit like $\mathrm{P} = \frac{9}{10}\pi$ is divided into 4 segments (3-2-2-3 revolution) or more to keep the diverging magnitude under 10^7 for all the segments.

Step 2: Orbit Connection with Control Maneuver

The separated segments are connected by the impulsive velocity change. The sufficient conditions to design the periodic orbits in the ER3BP have been described in Chapter 5. To satisfy the conditions initial velocity has to be fixed normal to xz-plane through the design process.

By virtue of the symmetry of the ER3BP about the apse line, the first and last segments show the symmetry trajectories obtained by backward propagation from the initial state for the last segment.

The intermediate segments are designed to bridge the terminal positions of the first segment and the last segment (see Figure 6.3). The target positions are simply located symmetry about the xz-plane (only the sign of y is opposite) since the first and last segments are symmetry about the xz-plne. Thus, when there is only one intermediate segment is given, it is also symmetry and this property reduces the design complexity.

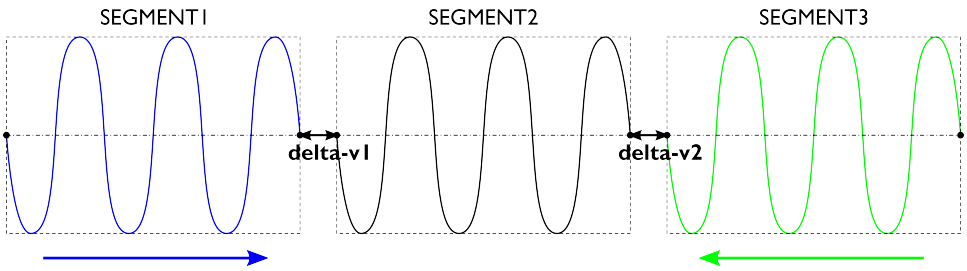

Figure 6.3: Illustration of the Orbits (segments) Connection

Step 3: Maneuver Free Orbit Connection This step searches the periodic natural orbit. The connected orbit designed in step2 requires the velocity change maneuver to construct the periodic orbit. The magnitude of the velocity change could be very small and negligible under small eccentricity model but it would not be assured in larger eccentricity model. This is because the connection position may not be appropriately given. Therefore, the required maneuvers are to be minimized by releasing the connection positions free nearby the reference orbit. In theory, the maneuver free orbit can be designed as a result of the short period orbit design that proves the periodic orbit can be exist also in the ER3BP.

This algorithm from step 1 to step 3 are summarized and is called RMSL (Recursive Multi-Step Linearization)[Ishii 1991] this method is effective for highly nonlinear design problem and the orbit around collinear L point is highly nonlinear and, furthermore, it is highly unstable. Hence, the RMSL method is practical for the period orbit design around L point.

The RMSL process has been done in a very small eccentricity and extrapolate to the larger eccentricity model. The effectiveness of this extrapolation has already been confirmed in the short period orbit design.

6.2.1 Formulation of RMSL

The coasting trajectory design is difficult in some cases like highly unstable trajectory. Trajectory connection is very useful to avoid the difficulty of the design problem.

The connected trajectory starts and returns to the given positions by permitting the midcourse impulsive velocity change. Then, the midcourse maneuver is brought to zero for coasting trajectory design. First, section 1 presents two trajectory connection. The whole sequence is divided into two segments assuming the intermediate connection position and each trajectory is designed independently. Next, section 2 shows three segments connections. The three trajectories connection requires two maneuvers and

both are to be zero.

6.2.1.1 Two-Trajectory Connection

This section presents the simplest trajectory connection (Figure 1). The objective is to design $\mathbf{r}_0$ to $\mathbf{r}_2$ trajectory in $2\mathrm{P}$ flight time. P represents the orbit period of each trajectory.

Initially intermediate connection position $\mathbf{r}_1$ and final position $\mathbf{r}_2$ are assumed of $\mathbf{r}_0$. Therefore, both two trajectories start and return at the position in same time duration P and the whole trajectory is a returning trajectory from/to $\mathbf{r}_0$ in $2\mathrm{P}$. Since this stage permits the velocity disagreement, a connection maneuver $\boldsymbol{\Delta}\mathbf{v}$ is required.

The required maneuver is:

$$\boldsymbol{\Delta}\mathbf{v} = \mathbf{v}_1^+ - \mathbf{v}_1^- \tag{6.1}$$

The initial displacement is transferred simply by the State Transition Matrix (STM). When the State Transition Matrix (STM) of the reference trajectory is described as $\boldsymbol{\Phi}_{\mathrm{i}}$.

$$\begin{bmatrix} \boldsymbol{\delta}\mathbf{r}_{\mathrm{f,i}} \\ \boldsymbol{\delta}\mathbf{v}_{\mathrm{f,i}} \end{bmatrix} = \boldsymbol{\Phi}_{\mathrm{i}} \begin{bmatrix} \boldsymbol{\delta}\mathbf{r}_{0,\mathrm{i}} \\ \boldsymbol{\delta}\mathbf{v}_{0,\mathrm{i}} \end{bmatrix} \tag{6.2}$$

where the subscript i represents the label of respective trajectory.

From the design condition, the Initial and final positions are fixed to $\mathbf{r}_0$. Initially, an intermediate connection position is also fixed to $\mathbf{r}_0$. However, the boundary is omitted to build the coasting trajectory.

Eq. 6.2 is transformed into specialized form depending on the design condition:

$$\begin{bmatrix} \boldsymbol{\delta}\mathbf{r}_{\mathbf{1}}^- \\ \boldsymbol{\delta}\mathbf{v}_{\mathbf{1}}^- \end{bmatrix} = \boldsymbol{\Phi}_{\mathbf{1}} \begin{bmatrix} \mathbf{0} \\ \boldsymbol{\delta}\mathbf{v}_{\mathbf{0}} \end{bmatrix} \tag{6.3}$$

$$\begin{bmatrix} \mathbf{0} \\ \boldsymbol{\delta}\mathbf{v}_{\mathbf{2}} \end{bmatrix} = \boldsymbol{\Phi}_{\mathbf{2}} \begin{bmatrix} \boldsymbol{\delta}\mathbf{r}_{\mathbf{1}}^+ \\ \boldsymbol{\delta}\mathbf{v}_{\mathbf{1}}^+ \end{bmatrix} \tag{6.4}$$

The $\boldsymbol{\delta}\mathbf{r}_1^+$ and $\boldsymbol{\delta}\mathbf{r}_1^-$ have to be equal in order to maintain the connection. The difference between resulting velocity gap is, then, updated required maneuver.

For the smooth connection, we want to set the updated velocity gap to be zero:

$$(\mathbf{v}_1^+ + \boldsymbol{\delta}\mathbf{v}_1^+) - (\mathbf{v}_1^- + \boldsymbol{\delta}\mathbf{v}_1^-) = 0 \quad (6.5)$$

$$(\mathbf{v}_1^+ - \mathbf{v}_1^-) + (\boldsymbol{\delta}\mathbf{v}_1^+ + \boldsymbol{\delta}\mathbf{v}_1^-) = 0 \quad (6.6)$$

Substituting Eq. 6.1 into Eq. 6.6 yields:

$$\boldsymbol{\delta}\mathbf{v}_1^+ + \boldsymbol{\delta}\mathbf{v}_1^- = -\boldsymbol{\Delta}\mathbf{v} \quad (6.7)$$

The $\boldsymbol{\delta}\mathbf{v}_1^+$ and $\boldsymbol{\delta}\mathbf{v}_1^-$ are given from Eqs. 6.19 and 6.20:

$$\boldsymbol{\delta}\mathbf{v}_1^- = \boldsymbol{\Phi}_{1,\mathrm{vv}}\boldsymbol{\Phi}_{1,\mathrm{rv}}^{-1}\boldsymbol{\delta}\mathbf{r}_1 \quad (6.8)$$

$$\boldsymbol{\delta}\mathbf{v}_1^+ = -\boldsymbol{\Phi}_{2,\mathrm{rv}}^{-1}\boldsymbol{\Phi}_{2,\mathrm{rr}}\boldsymbol{\delta}\mathbf{r}_1 \quad (6.9)$$

where $\boldsymbol{\Phi}_{\mathrm{i,j}}$ represent separated STM as;

$$\boldsymbol{\Phi}_{\mathrm{i}} = \begin{bmatrix} \boldsymbol{\Phi}_{\mathrm{i,rr}} & \boldsymbol{\Phi}_{\mathrm{i,rv}} \\ \boldsymbol{\Phi}_{\mathrm{i,vr}} & \boldsymbol{\Phi}_{\mathrm{i,vv}} \end{bmatrix} \quad (6.10)$$

In conclusion, the necessary position displacement at the connection is given by summarizing Eqs. 6.7, 6.8 and 6.9:

$$\boldsymbol{\delta}\mathbf{r}_1 = (\boldsymbol{\Phi}_{2,\mathrm{rv}}^{-1}\boldsymbol{\Phi}_{2,\mathrm{rr}} + \boldsymbol{\Phi}_{1,\mathrm{vv}}\boldsymbol{\Phi}_{1,\mathrm{rv}}^{-1})^{-1}\boldsymbol{\Delta}\mathbf{v} \quad (6.11)$$

The initial trajectory gives a velocity gap $\boldsymbol{\Delta}\mathbf{v}$ at the connection The obtained $\boldsymbol{\Delta}\mathbf{v}$ gives the position displacement to design coasting arc.

6.2.1.2 Thee-Trajectory Connection

The previous section shows the design method of coasting arc by canceling one midcourse impulsive maneuver from connected two trajectories. This section conduct the coasting trajectory design by similar method to two trajectory connection method.

At first, three position to position trajectories are designed from $\mathbf{r}_0$ to $\mathbf{r}_3$. The intermediate positions $\mathbf{r}_1$ and $\mathbf{r}_2$ are given. Since the $\mathbf{r}_1$ and $\mathbf{r}_2$ are selected arbitrary, the velocity gap happens two connection positions.

$$\boldsymbol{\Delta}\mathbf{v}_1 = \mathbf{v}_1^+ - \mathbf{v}_1^- \quad (6.12)$$

$$\boldsymbol{\Delta}\mathbf{v}_2 = \mathbf{v}_2^+ - \mathbf{v}_2^- \quad (6.13)$$

The STM of the designed three trajectories are then named similar rule as previous section, $\mathbf{\Phi}_1$, $\mathbf{\Phi}_2$ and $\mathbf{\Phi}_3$. Following the expression of Eq. 6.2, the differentials are obtained as;

$$\begin{bmatrix} \boldsymbol{\delta}\mathbf{r}_1^- \\ \boldsymbol{\delta}\mathbf{v}_1^- \end{bmatrix} = \mathbf{\Phi}_1 \begin{bmatrix} \boldsymbol{\delta}\mathbf{r_0} \\ \boldsymbol{\delta}\mathbf{v_0} \end{bmatrix} \tag{6.14}$$

$$\begin{bmatrix} \boldsymbol{\delta}\mathbf{r}_2^- \\ \boldsymbol{\delta}\mathbf{v}_2^- \end{bmatrix} = \mathbf{\Phi}_2 \begin{bmatrix} \boldsymbol{\delta}\mathbf{r}_1^+ \\ \boldsymbol{\delta}\mathbf{v}_1^+ \end{bmatrix} \tag{6.15}$$

$$\begin{bmatrix} \boldsymbol{\delta}\mathbf{r}_3 \\ \boldsymbol{\delta}\mathbf{v}_3 \end{bmatrix} = \mathbf{\Phi}_3 \begin{bmatrix} \boldsymbol{\delta}\mathbf{r}_2^- \\ \boldsymbol{\delta}\mathbf{v}_2^- \end{bmatrix} \tag{6.16}$$

In order to maintain the trajectory connection;

$$\boldsymbol{\delta}\mathbf{r}_1^+ = \boldsymbol{\delta}\mathbf{r}_1^- = \boldsymbol{\delta}\mathbf{r}_1 \tag{6.17}$$

$$\boldsymbol{\delta}\mathbf{r}_2^+ = \boldsymbol{\delta}\mathbf{r}_2^- = \boldsymbol{\delta}\mathbf{r}_2 \tag{6.18}$$

The initial and final positions are design parameters therefore the position displacement at the locations are fixed to zero. Hence, Eq. 6.14- 6.16 are re-formed as;

$$\begin{bmatrix} \boldsymbol{\delta}\mathbf{r}_1 \\ \boldsymbol{\delta}\mathbf{v}_1^- \end{bmatrix} = \mathbf{\Phi}_1 \begin{bmatrix} \mathbf{0} \\ \boldsymbol{\delta}\mathbf{v}_0 \end{bmatrix} \tag{6.19}$$

$$\begin{bmatrix} \boldsymbol{\delta}\mathbf{r}_2 \\ \boldsymbol{\delta}\mathbf{v}_2^- \end{bmatrix} = \mathbf{\Phi}_2 \begin{bmatrix} \boldsymbol{\delta}\mathbf{r}_1^+ \\ \boldsymbol{\delta}\mathbf{v}_1^+ \end{bmatrix} \tag{6.20}$$

$$\begin{bmatrix} \mathbf{0} \\ \boldsymbol{\delta}\mathbf{v}_3 \end{bmatrix} = \mathbf{\Phi}_3 \begin{bmatrix} \boldsymbol{\delta}\mathbf{r}_2^+ \\ \boldsymbol{\delta}\mathbf{v}_2^+ \end{bmatrix} \tag{6.21}$$

The midcourse maneuvers $\boldsymbol{\Delta}\mathbf{v}_1$ and $\boldsymbol{\Delta}\mathbf{v}_2$ are to be zero in order to have the coasting trajectory. Similar to two-trajectory connection, the required velocity changes are obtained by;

$$\boldsymbol{\delta}\mathbf{v}_1^+ + \boldsymbol{\delta}\mathbf{v}_1^- = -\boldsymbol{\Delta}\mathbf{v}_1 \tag{6.22}$$

$$\boldsymbol{\delta}\mathbf{v}_2^+ + \boldsymbol{\delta}\mathbf{v}_2^- = -\boldsymbol{\Delta}\mathbf{v}_2 \tag{6.23}$$

The $\boldsymbol{\delta}\mathbf{v}_1^-$ is simply calculated from Eq. 6.14:

$$\boldsymbol{\delta}\mathbf{v}_1^- = \boldsymbol{\Phi}_{1,\mathrm{vv}}(\boldsymbol{\Phi}_{1,\mathrm{rv}}^{-1}\boldsymbol{\delta}\mathbf{r}_1) \tag{6.24}$$

From Eq. 6.16 the $\boldsymbol{\delta}\mathbf{v}_2^+$ can be also given as:

$$\boldsymbol{\delta}\mathbf{v}_2^+ = -\boldsymbol{\Phi}_{3,\mathrm{rv}}^{-1}\boldsymbol{\Phi}_{3,\mathrm{rr}}\boldsymbol{\delta}\mathbf{r}_2 \tag{6.25}$$

Eq. 6.15 yields two equations. The $\boldsymbol{\delta}\mathbf{v}_1^+$ and $\boldsymbol{\delta}\mathbf{v}_2^-$ are affected from both the initial and final velocity changes.

$$\begin{aligned} \boldsymbol{\delta}\mathbf{v}_1^+ &= \boldsymbol{\Phi}_{2,\mathrm{rv}}^{-1}(\boldsymbol{\delta}\mathbf{r}_2 - \boldsymbol{\Phi}_{2,\mathrm{rr}}\boldsymbol{\delta}\mathbf{r}_1) \\ &= -\boldsymbol{\Phi}_{2,\mathrm{rv}}^{-1}\boldsymbol{\Phi}_{2,\mathrm{rr}}\boldsymbol{\delta}\mathbf{r}_1 + \boldsymbol{\Phi}_{2,\mathrm{rv}}^{-1}\boldsymbol{\delta}\mathbf{r}_2 \end{aligned} \tag{6.26}$$

$$\boldsymbol{\delta}\mathbf{v}_2^- = \boldsymbol{\Phi}_{2,\mathrm{vr}}\boldsymbol{\delta}\mathbf{r}_1 + \boldsymbol{\Phi}_{2,\mathrm{vv}}\boldsymbol{\delta}\mathbf{v}_1^+ \tag{6.27}$$

Substituting Eq. 6.26 into Eq. 6.27 yields;

$$\begin{aligned} \boldsymbol{\delta}\mathbf{v}_2^- &= \boldsymbol{\Phi}_{2,\mathrm{vr}}\boldsymbol{\delta}\mathbf{r}_1 + \boldsymbol{\Phi}_{2,\mathrm{vv}}[\boldsymbol{\Phi}_{2,\mathrm{rv}}^{-1}(\boldsymbol{\delta}\mathbf{r}_2 - \boldsymbol{\Phi}_{2,\mathrm{rr}}\boldsymbol{\delta}\mathbf{r}_1)] \\ &= (\boldsymbol{\Phi}_{2,\mathrm{vr}} - \boldsymbol{\Phi}_{2,\mathrm{vv}}(\boldsymbol{\Phi}_{2,\mathrm{rv}}^{-1}\boldsymbol{\Phi}_{2,\mathrm{rr}}))\boldsymbol{\delta}\mathbf{r}_1 + \boldsymbol{\Phi}_{2,\mathrm{vv}}(\boldsymbol{\Phi}_{2,\mathrm{rv}}^{-1}\boldsymbol{\delta}\mathbf{r}_2) \end{aligned} \tag{6.28}$$

Substituting Eqs. 6.24 - 6.26 and Eq. 6.28 into Eqs. 6.22 and 6.23 produces;

$$(\boldsymbol{\Phi}_{1,\mathrm{vv}}\boldsymbol{\Phi}_{1,\mathrm{rv}}^{-1} + \boldsymbol{\Phi}_{2,\mathrm{rv}}^{-1}\boldsymbol{\Phi}_{2,\mathrm{rr}})\boldsymbol{\delta}\mathbf{r}_1 - \boldsymbol{\Phi}_{2,\mathrm{rv}}^{-1}\boldsymbol{\delta}\mathbf{r}_2 = \boldsymbol{\Delta}\mathbf{v}_1 \tag{6.29}$$

$$(\boldsymbol{\Phi}_{2,\mathrm{vr}} - \boldsymbol{\Phi}_{2,\mathrm{vv}}(\boldsymbol{\Phi}_{2,\mathrm{rv}}^{-1}\boldsymbol{\Phi}_{2,\mathrm{rr}}))\boldsymbol{\delta}\mathbf{r}_1 + (\boldsymbol{\Phi}_{2,\mathrm{vv}}\boldsymbol{\Phi}_{2,\mathrm{rv}}^{-1} + \boldsymbol{\Phi}_{3,\mathrm{rv}}^{-1}\boldsymbol{\Phi}_{3,\mathrm{rr}})\boldsymbol{\delta}\mathbf{r}_2 = \boldsymbol{\Delta}\mathbf{v}_2 \tag{6.30}$$

Summarizing Eqs. 6.29 and 6.30 finally gives the solution for $\boldsymbol{\delta}\mathbf{r}_1$ and $\boldsymbol{\delta}\mathbf{r}_2$:

6.2.1.3 N–Trajectory Connection

Finally, this section makes generalization for the trajectory connection as N-trajectory connection algorithm. The sensitivity matrix of the position displacement is shown both in section 1 and section 2. Therefore, solving

the displacement analysis in same way, the sensitivity matrix for the N-trajectory connection is shown as:

$$\mathbf{\Delta V} = \begin{bmatrix} \mathbf{B}_1 & \mathbf{C}_1 & & & & \\ & \mathbf{A}_2 & \mathbf{B}_2 & \mathbf{C}_2 & & \\ \vdots & & & \ddots & & \vdots \\ & & & & \mathbf{A}_{n-1} & \mathbf{B}_{n-1} \end{bmatrix} \boldsymbol{\delta \mathbf{R}} \tag{6.31}$$

where

$$\mathbf{A}_n = -\mathbf{\Phi}_{n,vr} - \mathbf{\Phi}_{n,vv}(\mathbf{\Phi}_{n,rv}^{-1}\mathbf{\Phi}_{n,rr}) \tag{6.32}$$

$$\mathbf{B}_n = -\mathbf{\Phi}_{n+1,rv}^{-1}\mathbf{\Phi}_{n+1,rr} + \mathbf{\Phi}_{n,vv}\mathbf{\Phi}_{n,rv}^{-1} \tag{6.33}$$

$$\mathbf{C}_n = -\mathbf{\Phi}_{n+1,rv}^{-1} \tag{6.34}$$

6.3 Validation of Method

An initial estimated orbit requires 9-revolution. Figure 6.4 shows the propagated initial estimation in the ER3BP ($e = 1E^{-6}$). The orbit depart from the periodic motion and because of the large deviation plus the strong orbit divergence the direct differential correction does not work properly.

Through the step 1 the orbit is divided into 3 segments make up for 3-revolution trajectories. For this orbit, 3-revolution trajectory has in 10^5 magnitude of divergence. Hence, the stable differential correction can be expected. Figure 6.5 shows the propagated three separated segments of trajectories. The color definitions are same as in Figure 6.3. All trajectory of three segments are not deviate from the initial state and this makes the differential correction easier.

After the step 1 procedure the orbit terminal positions of each segment are corrected to be matched at same epoch (end of 1st and beginning of 2nd, end of 2nd and beginning of 3rd). Permitting the velocity difference, the segments are connected seamlessly. In result, the velocity gap become 0.01 mm/s for both between the first and second segments and second and last segments. The value seems negligible but Figure 6.4 shows it can not be.

Finally, by means of the the connection position optimization the periodic orbit design has been completed. Figure 6.6 shows the designed orbit.

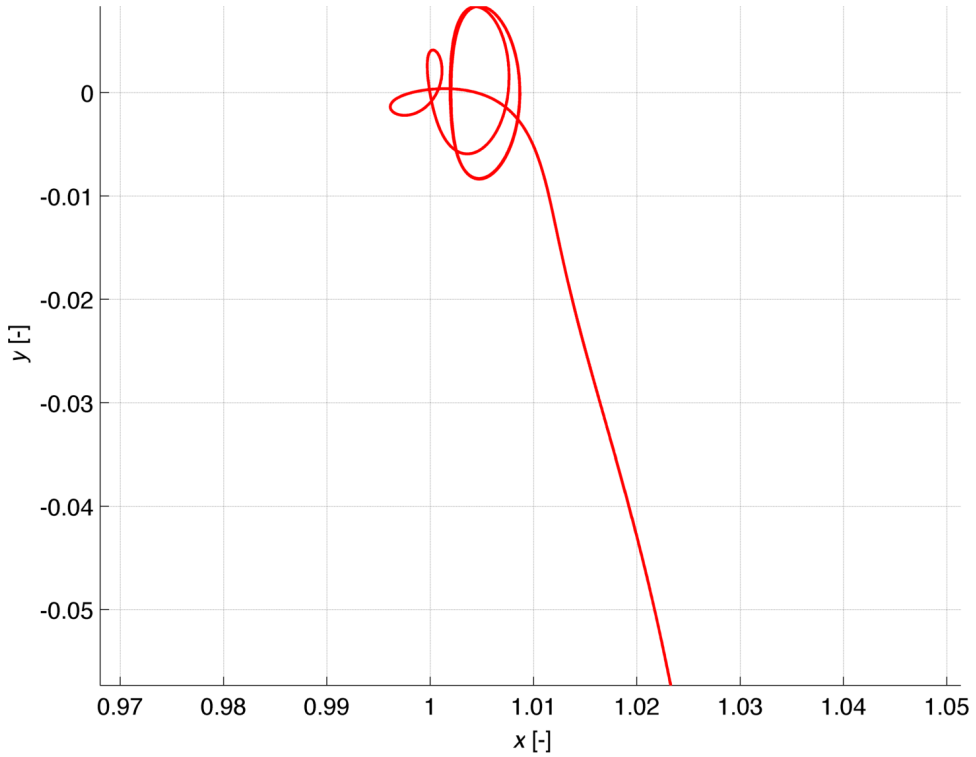

Figure 6.4: Continuous 9P Initial Estimated Trajectory

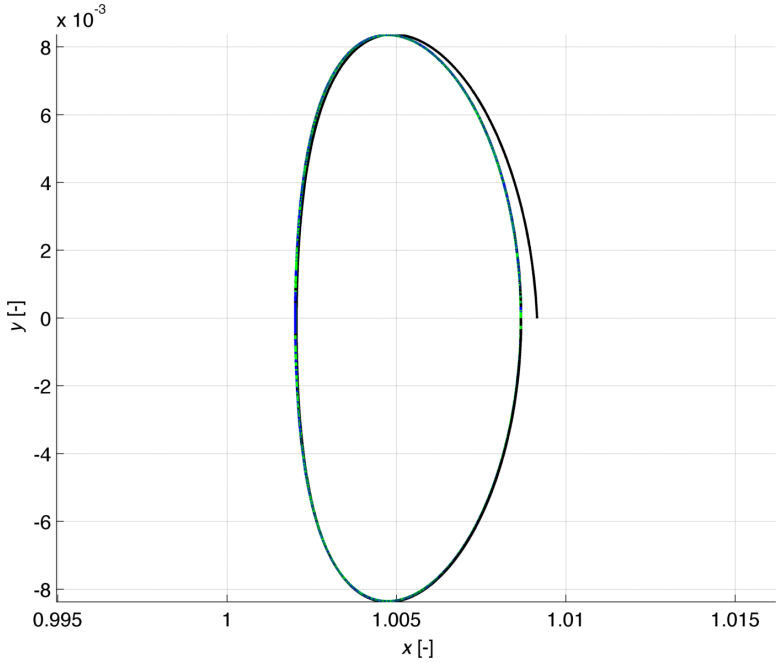

Figure 6.5: Three-Separated Segments

The every segment terminal patched seamlessly and naturally and the initial and terminal velocity vectors are perpendicular to xz-plane. Table 6.2 gives the modified initial conditions.

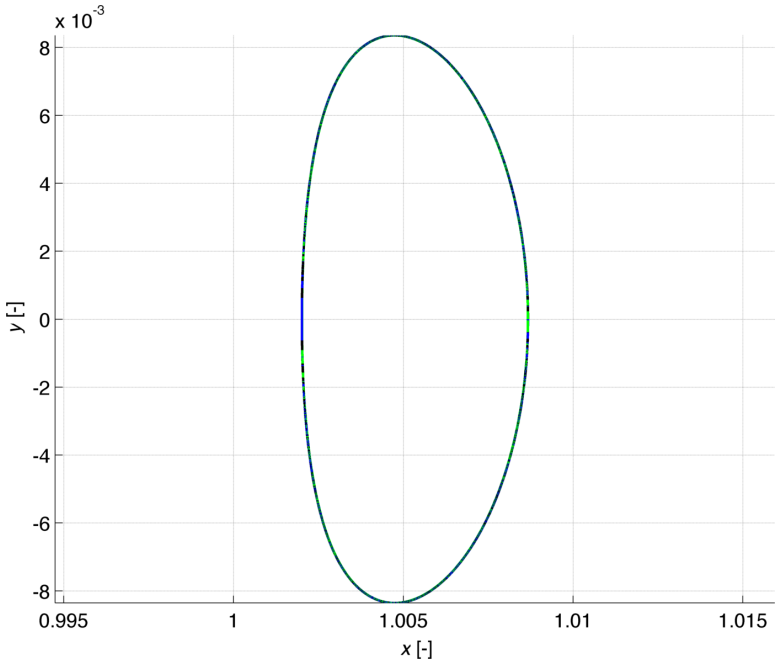

Figure 6.6: Long Period Orbit

Table 6.2: Initial Conditions of Long Period Orbit

Segment	Position	Velocity	Epoch (f)
FIRST	1.0087,0.0,0.0109	0.0,-0.0151,0.0	0.0
SECOND	1.0087,1.94E^{-8},0.0109	-1.96E^{-8},-0.0151,1.27^{-8}	8.378
LAST	1.0087,0.0,0.0109	0.0,-0.0151,0.0	0.0 (8π)

The periodic orbit design for the long period orbit has been done under small eccentricity model. Now the designed orbit is used for the extrapolation in larger eccentricity model. The relation of initial condition and eccentricity has been already shown in chapter 5. Therefore, we can select the arbitrary eccentricity and the relation give us the well approximated initial assumption. Without the assumption, the orbit design is forced to start from the widely apart trajectory like shown in Figure 6.4. An example of extrapolation is shown in Figure 6.7. The orbit is designed in $\mathrm{e} = 0.01$ model.

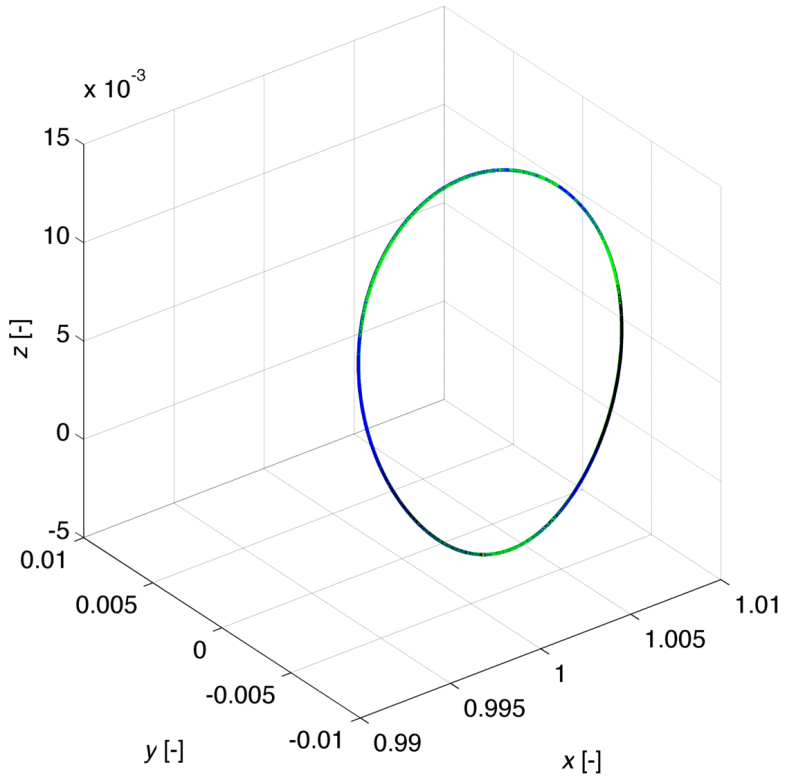

Figure 6.7: Long period orbit in large eccentricity model

The connection position optimization can be applied for more sensitive orbit. The $\mathrm{A_z} = 4.0 \times 10^5 [\mathrm{km}]$ Halo orbit has roughly 1400 of diverging magnitude. Thus, two-revolution is the maximum number of revolution to perform the differential correction well. For such orbit, the 12-revolution (6 segments connection) has been confirmed.

6.4 Practical size orbit design

The presented long period orbit ($\mathrm{P} = 8\pi/9$) shows the effectiveness of the method. However, the orbit is still not practical orbit for the normal L point mission since the orbit is still intermediate region between Earth and the L2. Therefore, for the usual mission use, $\mathrm{P} = 70\pi/71$ orbit will be shown. Figure 6.8 shows the reference Halo orbit (in CR3BP). The orbit size $\mathrm{A_z}$ is 3.5×10^5 which is within the range of usual size for the mission. In fact, SPICA which is planed by JAXA with international collaboration will be launched within the range from 3 to 4×10^5 km.

Considering the orbit period, $70\pi/71$, this orbit is required 71-revolution to satisfy the sufficient condition of periodic orbit design. Plus, the magni-

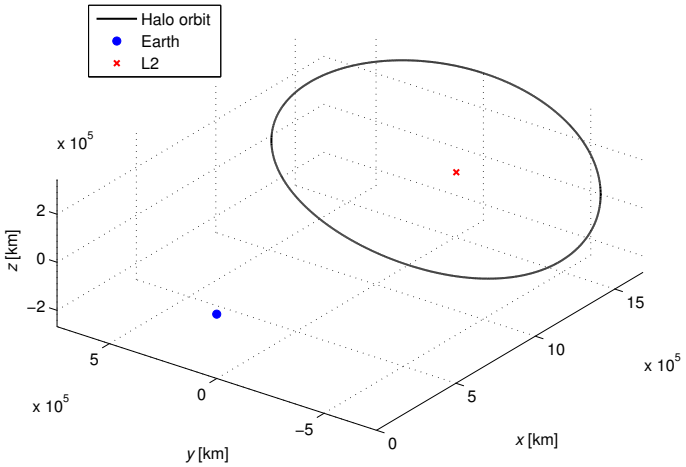

Figure 6.8: Example of practical size of Halo orbit

tude of orbit divergence over a period is around 1500. The periodic orbit is symmetry about the xz-plane and, therefore, 36-revolution designed orbit is simply compliment the latter 36-revolution (one revolution overlapped). Consequently, periodic orbit is designed conducting the RMSL method to find the coasting trajectory and keep the last orbit (36th orbit) symmetry about the xz-plane. Figure 6.9 present the periodic orbit designed in the realistic condition of Sun-Earth system that the eccentricity is 0.0167 and the secondary body mass is given by sum total of Earth and Moon at the Earth-Moon barycenter.

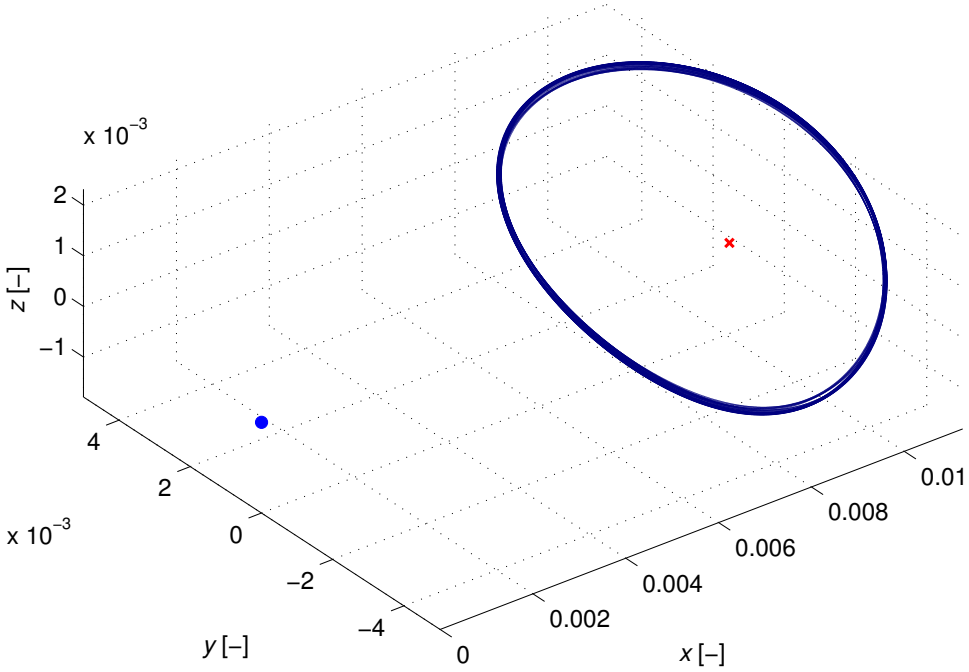

Figure 6.9: Periodic orbit (P = 70π/71) in Earth center ER3BP

CHAPTER 7

Orbit Maintenance under Realistic Condition

Contents

7.1 Description

The orbit maintenance maneuver using the DST is presented in Chapter 4 using a Halo orbit reference in the CR3BP model.This chapter applies the method to realistic model. The reference is periodic orbit designed in the ER3BP.

Similar approach was used for European Space Agency's (ESA) Herschel/Planck missions. [2011 Markus] The determined state vector is propagated until the initially planned maneuver interval with assumed correction maneuver Δv. The non-diverging trajectory is obtained and define the best maneuver to maintain the orbit stay close to the nominal orbit.

The periodic orbit in the ER3BP is not a single loop closed orbit but a number of revolution recurrence orbit. Therefore, the STM propagated over a revolution would not be the Monodromy matrix and there is no specific eigenspace of the reference orbit. In fast, the principal directions of a revolution and the next revolution orbit are slightly different even for a periodic orbit. However, if the STM is propagated until the orbit closed in the phase space. The matrix can be considered as the Monodromy matrix what gives the egenspace for the reference.

Depending on which direction the calculation uses, the correction method is separately presented. The local correction design propagate the

STM in a revolution and the global correction uses the Monodromy matrix to get the principal directions.

The followings show the correction result by using a reference 2:5 periodic orbit (Figure 7.1). The eccentricity of the ER3BP is defined as 0.01.

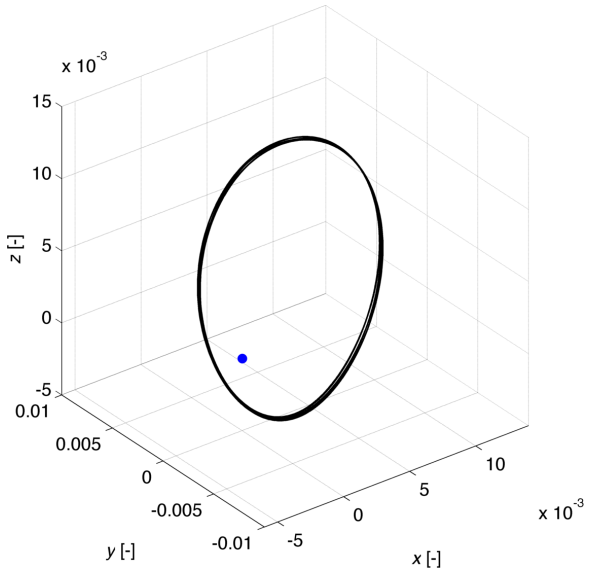

Figure 7.1: Illustration of Periodic Orbit Design Process

7.2 Local Correction

The libration orbits is highly unstable, therefore, the usual correction maneuver treat in the near term of diverging displacement. This local correction realizes the maneuver using the direction information of each revolution. The STMs are, then, propagated for each orbit separately. The diverging directions from five-revolution are presented in Table 7.1. The angle between previous orbit's direction are described in $\Delta\theta$. The $\Delta\theta$ shows how much angle the maximum stretching direction is twisted after a revolution. It is clear seen in the table the diverging directions changes the direction in each revolution.

7.3 Global Correction

The global correction method maintains the state differential in the long term. The reference STM is Monodromy matrix and the eigenvectors of the Monodromy matrix is used for the principal directions. Since the reference

Table 7.1: Local Directions of Reference Orbit

Orbit definition	Diverging direction	$\Delta\theta$ [°]
LOC1	[0.310,0.220,-0.008,0.572,-0.316,0.655]	0.60
LOC2	[0.320,0.211,-0.007,0.577,-0.322,0.644]	1.01
LOC3	[0.308,0.229,-0.009,0.567,-0.318,0.654]	1.50
LOC4	[0.317,0.223,-0.008,0.571,-0.321,0.649]	1.45
LOC5	[0.315,0.223,-0.008,0.571,-0.321,0.649]	0.96

orbit is a periodic orbit, the diverging displacement is nullified from the closed orbit by canceling the global diverging direction. This method does not treat the local direction and permits the displacement growth in the near term. Table 7.2 shows the global direction at each revolution. The Monodromy matrix is the STM propagated over whole trajectory, therefore, the diverging directions after the second revolution are ttransfered by multiplied with the STM. The angle ϕ presented in the last column represent the difference from the local direction at the time.

Table 7.2: Global Directions of Reference Orbit

Orbit definition	Diverging direction	ϕ [°]
GLO1	[0.315,0.223,-0.008,0.571,-0.323,0.648]	0.69
GLO2	[0.310,0.219,-0.008,0.571,-0.316,0.655]	1.08
GLO3	[0.319,0.212,-0.006,0.577,-0.321,0.646]	1.43
GLO4	[0.309,0.228,-0.009,0.567,-0.320,0.654]	1.38
GLO5	[0.316,0.210,-0.006,0.578,-0.316,0.650]	0.94

7.4 Discussion

The artificial state displacement is assumed as same manner as in Chapter 4 and the Δv are calculated as Eq. 4.16 and found the minimum number with Eqs. 4.21 and 4.22.

The error suppressing orbit correction maneuver (OCM) for assumed displacement is performed and summarized in Table 7.3 and 7.4.

LOCM and GOCM represent the Local OCM and Global OCM, respectively. The LOCM eliminates the stretching error from the state displace-

ment but the directions are not consistent at every maneuver. The GOCM takes out the diverging error instead of local maximum stretching direction. Thus, the magnitude of correction after GOCM2 becomes zero.

In summary, the superiority of the GOCM is shown in this section. In addition to that the correction magnitude is in proportional to the magnitude of diverging component included in the displacement (shown in chapter 4). Hence, the resulting correction magnitude is easily estimated for the other scale or direction of displacement.

Table 7.3: Local Correction Maneuver Results

Error direction	Magnitude of Correction Maneuver [$\times 10^{-3}$ m/s]					
	LOCM1	LOCM2	LOCM3	LOCM4	LOCM5	TOTAL
x	0.65	0.03	0.06	0.50	2.35	3.59
y	1.61	0.01	0.05	0.17	0.89	2.73
z	3.40	0.12	0.03	0.10	1.56	5.22
$\dot{x}$	0.82	0.01	0.02	0.09	0.47	1.41
$\dot{y}$	0.58	0.01	0.02	0.13	0.67	1.41
$\dot{z}$	0.02	0.01	0.03	0.03	0.02	0.06

Table 7.4: Global Correction Maneuver Results

Error direction	Magnitude of Correction Maneuver [$\times 10^{-3}$ m/s]					
	GOCM1	GOCM2	GOCM3	GOCM4	GOCM5	TOTAL
x	0.65	0.0	0.0	0.0	0.0	0.65
y	1.61	0.0	0.0	0.0	0.0	1.61
z	3.39	0.0	0.0	0.0	0.0	3.39
$\dot{x}$	0.82	0.0	0.0	0.0	0.0	0.82
$\dot{y}$	0.58	0.0	0.0	0.0	0.0	0.58
$\dot{z}$	0.02	0.0	0.0	0.0	0.0	0.02

CHAPTER 8

Conclusion and Remarks

In this thesis, trajectory design technique in Restricted Three-Body Problem (R3BP) have been presented around collinear Lagrangian point. The study consist of reference orbit design and feasible orbit maintenance method. The trajectory design is provided in Elliptic Restricted Three-Body Problem (ER3BP). The ER3BP is more actual model of the Restricted Three-Body Problem (R3BP) than commonly used Circular Restricted Three-Body Problem (CR3BP).

The periodic orbits in ER3BP are given as recurrent orbits unlike Halo orbits in the CR3BP whose recurrence cycle are arbitrary depending on the orbit period. We proposed two methods for the periodic orbit design in the ER3BP. The first is classical numerical differential method. Satisfying sufficient conditions by the initial condition modification construct the periodic orbits according to the symmetry of the model. The second is patching segments method. The whole orbit is separated into several segments and patched by impulsive velocity change. The each segment composed of specific number of revolution trajectories and the included number of revolution is defined based on the orbit diverging magnitude. The location of the connections are to be optimized to remove the velocity gap.

Orbit maintenance maneuver design using Dynamical Systems Theory (DST) has been studied for the periodic orbits in the ER3BP. The fundamental design idea is presented using a Halo orbit in the CR3BP. The principal subspaces are built by the invariant manifolds about the reference. The Halo orbit has only one subspace of diverging direction. Therefore, in order to maintain the error to be not deviating displacement, the diverging direction is suppressed from the assumed state error. In the ER3BP the local and global correction maneuvers are considered. By applying the DST periodic orbits in ER3BP have also principal directions but they are not identical subspaces. The local correction maintain the diverging direction obtained by diverging eigenvector of State Transition Matrix for each revolution. The global correction, however, treat the diverging direction obtained from diverging eigenvector of Monodromy matrix which is STM

over whole period of the orbit. The local correction nullifies the maximum error stretching direction but the direction will change in the next revolution. This results in that the local correction requires maneuvers in each revolution. The global correction cancel out the diverging direction over the period. Therefore, theoretically the one global correction avoid a number of correction maneuver. The effectiveness of the global correction has been shown compared with the local correction in terms of the total magnitude of velocity change.

APPENDIX A

State Transition Matrix

This section introduces the State Transition Matrix which enables the linear analysis of the state displacement from the reference trajectory.

The equation of motion like Eq. 2.19 are simply summarized as:

$$\dot{\mathbf{y}} = \mathrm{f}(\mathbf{y}) \tag{A.1}$$

where

$$\mathbf{y} = [\mathrm{x}, \mathrm{y}, \mathrm{z}, \dot{\mathrm{x}}, \dot{\mathrm{y}}, \dot{\mathrm{z}}] \tag{A.2}$$

Trajectories with a specific initial condition $\mathbf{y}_0$ is expressed by using flow map $\phi(\mathrm{t}; \mathbf{y}_0)$. Therefore, Eq. A.1 can be written as:

$$\frac{\mathrm{d}\phi(\mathrm{t}; \mathbf{y}_0)}{\mathrm{dt}} = \mathrm{f}(\phi(\mathrm{t}; \mathbf{y}_0)) \tag{A.3}$$

$$\phi(\mathrm{t}, \mathbf{y}_0) = \mathbf{y}_0 \tag{A.4}$$

When the initial condition $\mathbf{y}_0$ is slightly deviated as much as $\boldsymbol{\delta}\mathrm{y}_0$ (see Figure A.1), the state deviation at time t is given by:

$$\bar{\boldsymbol{\delta}}\mathrm{y}(\mathrm{t}) = \phi(\mathrm{t}; \bar{\mathbf{y}}_0 + \bar{\boldsymbol{\delta}}\mathrm{y}_0) - \mathrm{f}(\phi(\mathrm{t}; \bar{\mathbf{y}}_0)) \tag{A.5}$$

Expanding in a Taylor series yields:

$$\bar{\boldsymbol{\delta}}\mathrm{y}(\mathrm{t}) = \frac{\partial\phi(\mathrm{t}; \bar{\mathbf{y}}_0)}{\partial\bar{\mathbf{y}}_0}\bar{\boldsymbol{\delta}}\mathrm{y}_0 + \mathrm{higher-order} \tag{A.6}$$

Therefore, we can approximate the equation of relative motion by linearization at the reference when the size of the displacement is small magnitude. The matrix $\frac{\partial\phi(\mathrm{t}; \bar{\mathbf{y}}_0)}{\partial\bar{\mathbf{y}}_0}\bar{\boldsymbol{\delta}}\mathrm{y}_0$ that satisfies the above relation to first order is called the State Transition Matrix (STM). The state displacement at time t_1 is then obtained by initial deviation $\bar{\mathbf{y}}_0$ and STM from t_0 to t_1, $\Phi(\mathrm{t}_1, \mathrm{t}_0)$ as:

$$\delta\bar{\mathbf{y}}(\mathrm{t}_1) = \Phi(\mathrm{t}_1, \mathrm{t}_0)\delta\bar{\mathbf{y}}_0 \tag{A.7}$$

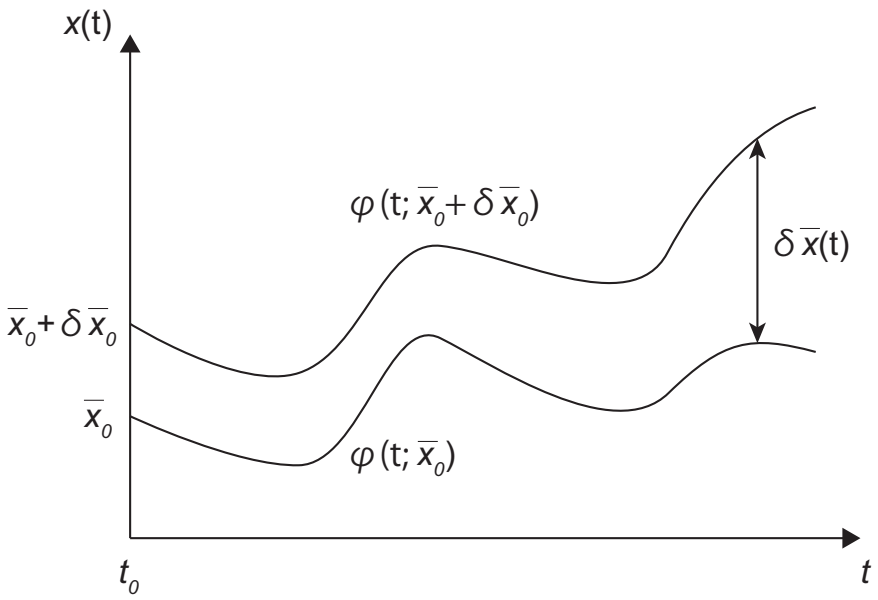

Figure A.1: Flow Map of Reference and a Neighboring Trajectory

Eq. A.7 is the solution to the linearized variational equation of Eq. A.1 as:

$$\dot{\bar{\mathbf{y}}}(\mathrm{t}) = \mathrm{Df}(\bar{\mathbf{y}}(\mathrm{t}))\bar{\boldsymbol{\delta}}\mathrm{y} \tag{A.8}$$

Since this is the linearized equation, $\mathrm{Df}(\bar{\mathbf{y}}(\mathrm{t}))$ is the Jacobian matrix of the flow function f along the reference trajectory. Consequently, obtained STM along the reference trajectory is useful in trajectory correction and modification.

In the CR3BP and the ER3BP equation of motions, the Jocibian matrix is:

$$\mathrm{Df}(\bar{\mathbf{y}}(\mathrm{t})) = \begin{bmatrix} \mathbf{0} & \mathbf{I} \\ \boldsymbol{\Psi} & 2\boldsymbol{\Omega} \end{bmatrix} \tag{A.9}$$

where,

$$\boldsymbol{\Omega} = \begin{bmatrix} 0 & 1 & 0 \\ -1 & 0 & 0 \\ 0 & 0 & 0 \end{bmatrix} \tag{A.10}$$

$$\boldsymbol{\Psi} = \begin{bmatrix} \mathrm{Uxx} & \mathrm{Uxy} & \mathrm{Uxz} \\ \mathrm{Uyx} & \mathrm{Uyy} & \mathrm{Uyz} \\ \mathrm{Uzx} & \mathrm{Uzy} & \mathrm{Uzz} \end{bmatrix} \tag{A.11}$$

and $\mathbf{I}$ is the identity matrix.

It is important to know that the pseudo potential U of the CR3BP and ER3BP are different each other (see Eq. 2.42) the resulting STM in ER3BP from the same initial condition does not consistent with STM in the CR3BP.

Bibliography

[Broucke 1969] R. Broucke. *Stability of Periodic Orbits in the Elliptic Restricted Three-Body Problem*. AIAA Journal, vol. 7, no. 6, 1969. (Cited on page 5.)

[Campagnola 2008] S. Campagnola, M.W. Lo and P Newton. *Subregions of Motion and Elliptic Halo Orbits in the Elliptic Restricted Three-Body Problem*. AAS/AIAA Space Flight Mechnics Meeting, no. AAS 08-200, February 2008. (Cited on page 5.)

[Dunham 2001] D.W. Dunham and C.E. Roberts. *Stationkeeping Techniques for Libration-Point Satellites*. Journal of the Astronautical Sciences, vol. 49, no. 1, 2001. (Cited on page 3.)

[Faquhar 1968] R.W. Faquhar. *The Control and Use of Libration-Point Satellites*. PhD thesis, Stanford University, 1968. (Cited on page 2.)

[Hamasaki 2013] T. Hamasaki and J. Kawaguchi. *Solar Sail Trajectory Design for Exploration of Asteroid from/to Space Port around L2 Point*. AAS/AIAA Astrodynamics Specialist Conference, no. AAS 13-940, August 2013. (Cited on page 2.)

[Ikenaga 2011] T. Ikenaga and M Utashima. *Study on Stationkeeping Strategy for Libration Point Mission*. The 28th International Symposium on Space Technology and Science, no. 2011-d-60, June 2011. (Cited on page 28.)

[Ishii 1991] N. Ishii, J. Kawaguchi and H. Matsuo. *Design of multi-body Lamber type orbits specified departure and arrival positions*. In Montreal International Astronautical Federation Congress. IAF, October 1991. (Cited on page 49.)

[K.C. 1984] Howell K.C. *Three-Dimensional Periodic Halo Orbits*. Celestial Mechanics, vol. 32, no. 1, page 53, 1984. (Cited on page 2.)

[K.C. 1993] Howell K.C. and H.J. Pernicka. *Stationkeeping Method for Libration Point Trajectories*. Journal of Guidance, Control, and Dynamics, vol. 16, no. 1, 1993. (Cited on page 3.)

[K.C. 2001] Howell K.C. *Families of Orbits in the Vicinity of the Collinear Libration Points*. The Journal of the Astronautical Sciences, vol. 49, no. 1, 2001. (Cited on page 21.)

[Koon 1999] W.S. Koon, M.W. Lo, J.E. Marsden and S.D. Ross. *The Genesis Trajectory and Heteroclinic Connections*. AAS/AIAA Astrodynamics Specialist Conference, August 1999. (Cited on page 4.)

[Koon 2000] W.S. Koon, M.W. Lo, J.E. Marsden and S. Ross. *Heteroclinic Connections Between Periodic Orbits and Resonance Transitions in Celestial Mechanics*. Chaos, vol. 10, no. 2, pages 427–469, 2000. (Cited on page 4.)

[Nakamiya 2010] M. Nakamiya and Y. Kawakatsu. *Preliminary Study on Orbit Maintenance of Halo Orbits under Continuous Disturbance*. AAS/AIAA Space Flight Mechnics Meeting, no. AAS-10-119, February 2010. (Cited on page 4.)

[Nakamiya 2011] M. Nakamiya and Y. Kawakatsu. *A Study of the Transfers to the Quasi-halo Orbits using the characteristic of teh Dynamical System*. The 28th International Symposium on Space Technology and Science, no. 2011-d-60, June 2011. (Cited on page 4.)

[Sarris 1989] E. Sarris. *Families of Symmetric-Periodic Orbits in the Elliptic Three-Dimensional Three-Body Problem*. Astrophisics and Space Science, vol. 162, no. 1, 1989. (Cited on page 5.)

[Scheeres 2003] D.J. Scheeres, F.-Y Hsiao and Vinh N.X. *Stabilizing Motion Relative to an Unstable Orbit: Applications to Spacecraft Formation Flight*. Journal of Guidance, Control, and Dynamics, vol. 26, no. 1, 2003. (Cited on page 3.)

[Simanjuntak 2013] T. Simanjuntak. *Design of Loose Spacecraft Formation Flying around Halo Orbits*. PhD thesis, The Graduate University for Advanced Studies, 2013. (Cited on page 26.)

[Szebehely 1967] V. Szebehely. Theory of orbits; the restricted problem of three bodies. Academic Press, New York, 1967. (Cited on page 5.)

Trajectory Design for Lagrange Point Missions using DST in Restricted Three–Body Problem

–Abstruct–

This thesis investigates orbit maintenance of periodic orbits around a collinear Lagrange point in Elliptic Restricted Three-Body Problem (ER3BP) that includes the eccentricity of co-orbiting dominant two bodies. Since the ER3BP is higher fidelity dynamic model than commonly used Circular Restricted Three-Body Problem (CR3BP), the designed orbit in the ER3BP gives a realistic initial condition. The application of the Dynamical Systems Theory (DST) impulsive velocity correction is performed to cancel out the stretching displacement, which is obtained using the eigenvalue problem of the State Transition Matrix, from the reference orbit. The maneuver stabilizes the determined state displacement. Also the periodic orbits have been designed numerically by differential correction and Recursive Multi-Step Linearization (RMSL) method. The RMSL method can avoid the difficulty of the long ballistic trajectory design by means of the trajectory separation into multiple segments. Those results are verified in actual dynamic model using real ephemerides.

In the ER3BP, the period of particle's motion has to be synchronized with the primaries orbital period because of the time dependency of model. On the other hand, the orbit around collinear Lagrange points are highly unstable and the periodic orbit design problem is not so straight forward when the orbit period becomes very long. The RMSL method is an alternative method to multiple shooting method to eliminate the velocity gap to design a ballistic trajectory. The whole period is divided into multiple segments and enables linear analysis along the trajectory for each divided segment and the velocity disagreements generated by the separation are then minimized within a sufficient tolerance. The RMSL method gives any length of the periodic orbit once the dynamics are briefly provided.

The feasible maintenance maneuver design comes out from the loosing the control constraints. The diverging subspace is only error stretching direction in the state displacement. Therefore, when the diverging component is nullified, the deviation will not increase and stay around the reference trajectory. The idea is that only the diverging displacement in the orbit deviation is canceled out by the impulsive velocity correction to stabilize the motion nearby the reference trajectory. However, the periodic orbits in the ER3BP are closed in the phase space with the multi-revolution

and the maximum error stretching direction may change in every revolution. Therefore, the correction methods are described as Local and Global corrections depending on the correction target of the error stretching direction. The Local correction method define the correction target based on the STM propagated in a specific correction time interval and the Global correction method is taking account the diverging direction obtained from the Monodromy matrix.